

COPYRIGHT WARNING

This paper is protected by copyright. You are advised to print or download **ONE COPY** of this paper for your own private reference, study and research purposes. You are prohibited having acts infringing upon copyright as stipulated in Laws and Regulations of Intellectual Property, including, but not limited to, appropriating, impersonating, publishing, distributing, modifying, altering, mutilating, distorting, reproducing, duplicating, displaying, communicating, disseminating, making derivative work, commercializing and converting to other forms the paper and/or any part of the paper. The acts could be done in actual life and/or via communication networks and by digital means without permission of copyright holders.

The users shall acknowledge and strictly respect to the copyright. The recitation must be reasonable and properly. If the users do not agree to all of these terms, do not use this paper. The users shall be responsible for legal issues if they make any copyright infringements. Failure to comply with this warning may expose you to:

- Disciplinary action by the Vietnamese-German University.
- Legal action for copyright infringement.
- Heavy legal penalties and consequences shall be applied by the competent authorities.

The Vietnamese-German University and the authors reserve all their intellectual property rights.





DRIVING AND STEERING SYSTEM FOR AGRICULTURAL UGV

BACHELOR THESIS

BINH DUONG 2023



Submitted by: Le Thanh Thai

RUB Student ID: 19220663

VGU Student ID: 15375

Supervisor: Dr. Hien Vo

Co-supervisor: Mr. Duyen Do

Table of contents

1	Introduction	9
1.1	Problem statement, motivation	9
1.1.1	Problem.....	9
1.1.2	Motivation	9
1.2	Scope of the thesis	10
2	Fundamental and state of research	11
2.1	Factors affecting off-road vehicle performance.....	11
2.2	Motion resistance of vehicle running gear.....	11
2.2.1	Resistance due to wheel–terrain interaction	11
2.2.1.1	Rigid wheel–terrain interaction.....	11
2.2.1.2	Flexible tire–terrain interaction.....	13
2.2.1.3	Prediction of the operating mode of a pneumatic tire	14
2.2.2	Resistance due to tire flexing	15
2.3	Steering kinetics.....	16
2.3.1	Steering resistance.....	16
2.3.2	Ackermann steering geometry.....	18
3	Requirement determination.....	20
3.1	Functional requirement	20
3.2	Functional requirement evaluation	21
4	Development and selection	22
4.1	Concept	22
4.2	Concept evaluation	23
5	Implement of the chosen concept.....	24
5.1	Land properties	24
5.2	General design	25
5.3	Driving kinetics.....	26
5.3.1	General.....	26
5.3.2	Motion resistance.....	27
5.3.2.1	Bike wheel R_{bike}	27
5.3.2.2	Trolley wheel T_{rolley}	28
5.4	Steering kinetics.....	29
5.4.1	Steering geometry.....	29

5.4.1.1	Steering radius estimation	29
5.4.2	Steering resistance moment	30
6	Manufacturing.....	32
6.1	Motor and transmission	32
6.1.1	Required motor power	32
6.1.2	Motor choosing.....	32
6.1.3	Transmission system	36
6.2	Steering mechanism.....	38
6.2.1	DC electric cylinder.....	39
6.2.2	DC electric cylinder requirement	40
6.3	Control system	42
6.3.1	Control system overview	42
6.3.2	Input components	43
6.3.3	PLC wiring	45
6.4	Components list	46
6.5	Experiment.....	49
6.5.1	Driving experiment.....	50
6.5.2	Steering experiment.....	50
7	Conclusion.....	56



List of figures

Figure 1.1 Scope	10
Figure 2.1 Major external forces acting on a wheeled vehicle	11
Figure 2.2 Simplified wheel–soil interaction model	12
Figure 2.3 Flexible tire–terrain interaction.....	13
Figure 2.4 Behavior of a tire in the rigid and elastic operating modes.....	15
Figure 2.5 Stress distribution for in steering wheel [4]	16
Figure 2.6 Vehicle turning in a Pro-Ackerman condition	19
Figure 3.1 Functional requirement	21
Figure 5.1 Vegetable plot	24
Figure 5.2 General design side view	25
Figure 5.3 General design top view.....	25
Figure 5.4 General forces	26
Figure 5.5 Theoretical steering model.....	30
Figure 5.6 General steering design.....	30
Figure 6.1 300W motor	35
Figure 6.2 Transmission system side view (left) and back view (right).....	36
Figure 6.3 Transmission diagram.....	36
Figure 6.4 Sprocket size nomenclature.....	37
Figure 6.5 Chain sprocket RS40-10TB	38
Figure 6.6 General design.....	38
Figure 6.7 A 12V DC electric cylinder.....	39
Figure 6.8 Straight going.....	40
Figure 6.9 Turning right	40
Figure 6.10 Turning left	40
Figure 6.11 Electric cylinder stroke	41
Figure 6.12 Control system overview	42
Figure 6.13 Siemens S7-1500 PLC	42
Figure 6.14 Input module	43
Figure 6.15 FlySky FS-TH9X	43
Figure 6.16 Receiver FS-iA10B	44
Figure 6.17 PLC wiring	45
Figure 6.18 DC motor controller 1 (left) and 2 (right)	45
Figure 6.19 Design overview.....	46

Figure 6.20 Prototype	46
Figure 6.21 Straight driving testing	50
Figure 6.22 Experiment steering angle	51
Figure 6.23 1st steering experiment	52
Figure 6.24 2nd steering experiment	53
Figure 6.25 3rd steering experiment	54

List of tables

Table 3.1 Functional requirement evaluation	21
Table 4.1 Options table.....	22
Table 4.2 Concept 1 – level basic.....	22
Table 4.3 Concept 2 – level basic.....	22
Table 4.4 Concept 3 – level intermediate	22
Table 4.5 Concept 4 – level advance	23
Table 4.6 Concept evaluation	23
Table 5.1 Sandy loam specification.....	24
Table 5.2 UGV specifications	25
Table 6.1 Motor type comparison	33
Table 6.2 Estimating the steering radius from experiment.....	54

Abstract

This thesis presents a comprehensive investigation on the design and development of a highly efficient driving and steering system for an Unmanned Ground Vehicle (UGV) suitable for agricultural use. The primary objective of this research is to identify the optimal motor torque required for seamless and cost-effective movement and steering on deformable agricultural terrain. To achieve this goal, the methodology involves analyzing the interaction between the wheels and the terrain, and the results of the study are utilized to develop a prototype UGV. The thesis concludes by presenting the performance results of the prototype and offering suggestions for future enhancements. The work presented in this thesis is a valuable contribution to the development of UGVs for agriculture and has the potential to enhance the efficiency and effectiveness of farming operations.

1 Introduction

1.1 Problem statement, motivation

1.1.1 Problem

Due to growing concerns about environmental degradation, including polluted air, acid rain, and contaminated water sources, there has been a move towards more environmentally friendly methods of agriculture. The traditional, heavily mechanized style of agriculture has been seen as a contributor to these problems, as well as urbanization and industrialization, despite its benefits for large-scale production and improved farming procedures. In response, the agriculture industry is promoting a "green and modern" revolution, which seeks to minimize the environmental impact of agriculture while also making use of effective and easy-to-use technologies. This shift marks another evolution in agriculture, incorporating not only new technologies but also new ways of thinking about production. The focus is not only on maximizing output, but also on doing so in an environmentally responsible manner.

1.1.2 Motivation

As the global population reaches 7.5 billion, it is essential that the farming industry is able to produce enough food to meet the demand, while also being economically and environmentally sustainable. One solution to this challenge is the development of automated agriculture, which combines robotics, mechanical design, and automated control devices. Companies are investing in innovations such as drones, automatic tractors, harvesting machines, and watering and seeding robots to improve the farming process. The adoption of farm automation is becoming increasingly common among traditional agricultural companies.

In Vietnam, agriculture remains an important sector of the economy, despite a decreasing share due to economic restructuring. The agricultural sector provides jobs for many workers and contributes to the country's exports, including rice, coffee, cotton yarn, peanuts, rubber, sugar, and tea. However, the agricultural sector in Vietnam also faces many difficulties, including a fragmented and small-scale organization, and the impact of climate change. To address these challenges, tracking crops on farms is vital for improving productivity and dealing with the unpredictable climate. Automated agriculture has been on the rise in recent years to increase food efficiency and safety, as well as to collect real-time data on crop growth and development. The use of automation in the seedling stage of crop care can provide precise and timely information, while reducing the time and effort required for manual monitoring.

1.2 Scope of the thesis

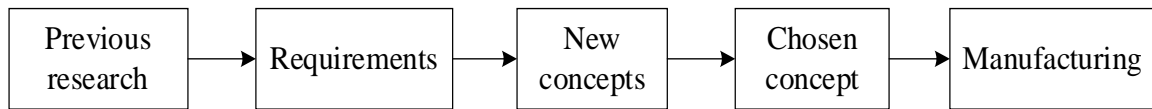


Figure 1.1 Scope

This project aims to create a device that can move over a vegetable bed and have sensors in the center to gather data. Initially, the focus will be on constructing the base so that the device can be controlled with a handheld controller. Later on, advanced features such as automatic scrolling will be added. The project is centered around designing the frame and the moving mechanism of the Unmanned Ground Vehicle (UGV). The goal is to build a prototype and test it.

The idea for the thesis was inspired by the flexibility and ease of use of UGV vehicles, particularly in the farming environment. A list of requirements for the system, including the drive part, design, and manufacturing conditions, is analyzed to ensure the work is precise and unambiguous. Previous research and existing products are thoroughly reviewed to make further progress. Each design is evaluated based on technical and economic criteria, and the best candidate is chosen for implementation.


Vietnamese-German University

Before creating a physical prototype, the system's features are designed in a virtual environment using the CAD program Solidworks 2022. The design is continuously improved and refined until the final product's attributes meet the desired specifications.

2 Fundamental and state of research

2.1 Factors affecting off-road vehicle performance

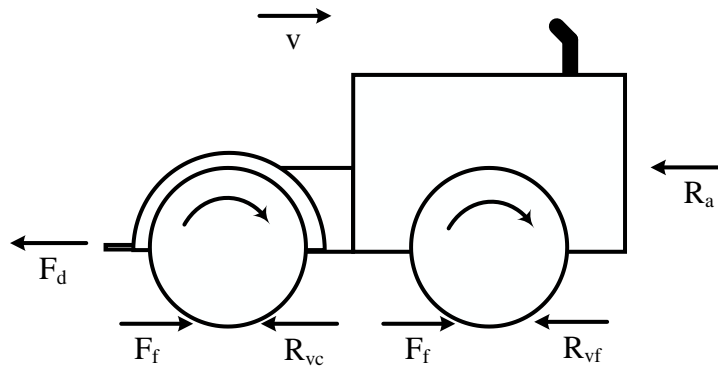


Figure 2.1 Major external forces acting on a wheeled vehicle

The major external forces acting on an off-road wheeled vehicle are shown in Figure 2.1. In the longitudinal direction. The equation of motion along the longitudinal direction is expressed by Eqn 2.1 [1].

$$ma = \frac{W}{g} a = F - R_a - R_v - F_d \mp W \sin \theta_s = F - R_a - R_v - F_d \mp R_g$$



Vietnamese-German University

Eqn 2.1

Symbol	Parameter and unit
R_a	aerodynamic resistance (N)
R_v	the motion resistance acting on the vehicle wheel (N)
F	thrust, tractive effort or propelling force (N)
F_d	drawbar pull (N)
θ_s	a slope at an angle to the horizontal which the vehicle operates on (degree)
m, W	vehicle mass and weight (kg)
a	the linear acceleration of the mass center along the longitudinal direction (m/s^2)

2.2 Motion resistance of vehicle running gear

2.2.1 Resistance due to wheel–terrain interaction

2.2.1.1 Rigid wheel–terrain interaction

The resistance due to wheel terrain interaction is come from compaction resistance which is calculated by Eqn 2.2 [2].

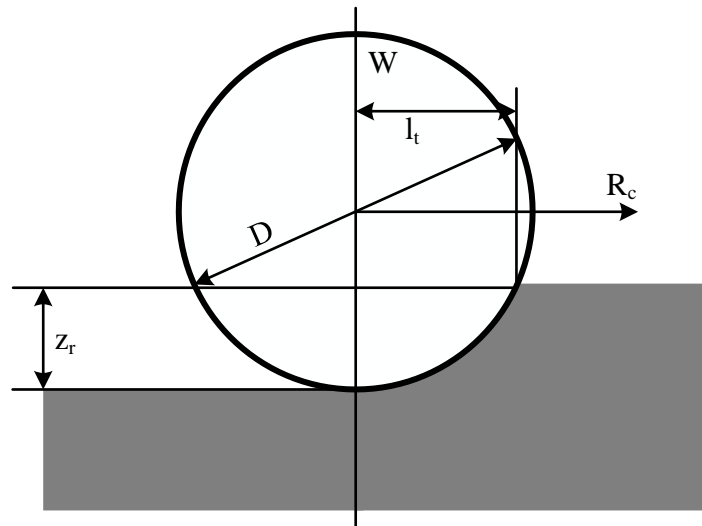


Figure 2.2 Simplified wheel–soil interaction model

$$R_c = \frac{1}{(3-n)^{\frac{2n+2}{2n+1}}(n+1)b_{ti}^{\frac{1}{2n+1}}\left(\frac{k_c}{b} + k_\phi\right)^{\frac{1}{2n+1}}\left(\frac{3W}{\sqrt{D}}\right)^{\frac{2n+2}{2n+1}}}$$

Eqn 2.2

The smaller dimension of the contact patch of the wheel b can be b_{ti} or l_t . To define l_t or b_{ti} is smaller, the following step will be done. First calculate the sinkage z using Eqn 2.3, then calculate the length l_t from Figure 2.2 using Eqn 2.4 [2].

$$z_r = \left(\frac{3W}{b_{ti}(3-n)\left(\frac{k_c}{b_{ti}} + k_\phi\right)\sqrt{D}} \right)^{\frac{2}{2n+1}}$$

Eqn 2.3

$$l_t = \sqrt{\left(\frac{D}{2}\right)^2 - \left(\frac{D}{2} - z_r\right)^2}$$

Eqn 2.4

Symbol	Parameter and unit
R_c	compaction resistance (N)
n	sinkage exponent of the soil
k_c	cohesive modulus of the soil
k_ϕ	frictional modulus of the soil
b_{ti}	wheel width (m)
W	vertical load on the wheel (N)
D	wheel diameter (m)
b	the smaller dimension of the contact patch of the wheel (b_{ti} or l_t)
l_t	contact length (m)
z_r	wheel sinkage (m)

2.2.1.2 Flexible tire–terrain interaction

When the tire pressure of a pneumatic tire is insufficient, and the ground is relatively solid, the tire will experience deformation..

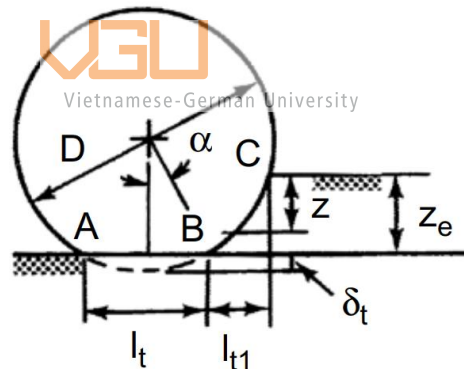


Figure 2.3 Flexible tire–terrain interaction

In this situation, it is reasonable to assume that the bottom part of the tire in contact with the ground, represented by section AB in the figure, is flattened. As a result, the pressure on the flat section of the tire that is in contact with the ground is equal to the inflation pressure (p_i) plus the pressure resulting from the stiffness of the tire carcass (p_c). Eqn 2.5. The tire manufacturer typically provides a "generalized deflection chart," which can be used to calculate the average ground pressure (p_g) for a specific tire with a given load and inflation pressure. [3].

$$p_g = p_i + p_c$$

Eqn 2.5

In this situation the compaction resistance is calculate by Eqn 2.6, where z_e is the sinkage of flexible tire Eqn 2.7 [3].

$$R_c = b_{ti} \left[\left(\frac{k_c}{b} + k_{\phi} \right) \frac{z_e^{n+1}}{n+1} \right]$$

Eqn 2.6

$$z_e = \left(\frac{p_g}{\frac{k_c}{b} + k_{\phi}} \right)^{\frac{1}{n}}$$

Eqn 2.7

If l_t is greater than the tyre width b_{ti} , then b_{ti} is the smaller dimension of the contact patch. On the other hand, if l_t is smaller than the tire width b_{ti} , then l_t is the smaller dimension of the contact patch. l_t is calculated in Eqn 2.8 [3].

$$l_t = \frac{W}{b_{ti} p_g}$$

Eqn 2.8

Symbol	Parameter and unit
z_e	sinkage of a flexible tire
p_i	inflation pressure
p_c	tire carcass pressure
p_g	average ground pressure

2.2.1.3 Prediction of the operating mode of a pneumatic tire

The behavior of a pneumatic tire with a certain load can vary between a rigid wheel, also known as the rigid mode of operation, and significant deflection, which is called the elastic mode of operation. The deflection is influenced by the tire's rigidity and the conditions of the terrain.

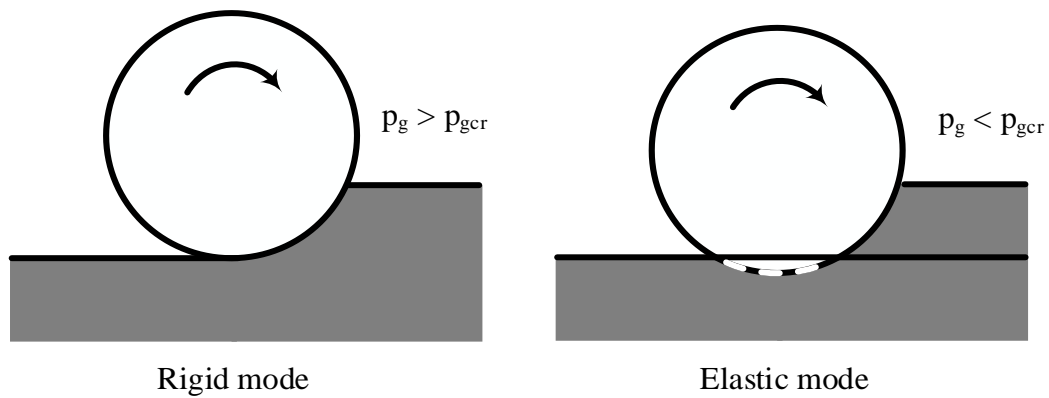


Figure 2.4 Behavior of a tire in the rigid and elastic operating modes

p_{gcr} is the critical ground pressure, above which the tire will behave like a rigid wheel. In another word, if p_g is greater than p_{gcr} then the tyre is assumed to be in the rigid mode of operation. On the other hand, if the value of p_g is less than p_{gcr} the tyre is assumed to be in the elastic mode of operation. p_{gcr} can be calculated by Eqn 2.9 (b is same as in the Eqn 2.6) [3]

$$p_{gcr} = \left[\frac{k_c}{b} + k_\phi \right]^{\frac{1}{2n+1}} \left[\frac{3W}{(3-n)b_{ti}\sqrt{D}} \right]^{\frac{2n}{2n+1}}$$

Eqn 2.9

2.2.2 Resistance due to tire flexing



Vietnamese-German University

When a tire experiences significant deflection, energy is lost not only due to compaction resistance but also due to the flexing of the tire material while it is rolling. As a result, a force that opposes the tire's motion, called the tire flexing resistance R_f , is generated in Eqn 2.10 [3].

$$R_f = \frac{3.581b_{ti}D^2p_g\varepsilon(0.0349\alpha \sin\alpha - \sin 2\alpha)}{\alpha(D - 2\delta_t)}$$

Eqn 2.10

where b_{ti} is tire width, D is tiring diameter, p_g is the average ground pressure, δ_t is tire deflection, as shown in Figure 2.3, and ε and α are determined as follows [3].

$$\alpha = \frac{D - 2\delta_t}{D}$$

Eqn 2.11

$$\varepsilon = 1 - \exp \left(-k_e \frac{\delta_t}{h} \right)$$

Eqn 2.12

where α is the contact angle shown in Figure 2.3 in degrees, h is tire section height, and the value of coefficient k_e is related to tire construction, its value is 15 for bias-ply tires and 7 for radial-ply tires [3].

Symbol	Parameter and unit
R_f	tire flexing resistance
α	contact angle shown in Figure 2.3 in degrees
δ_t	tire deflection
k_e	coefficient k_e is related to tire construction
h	tire section height

2.3 Steering kinetics

2.3.1 Steering resistance

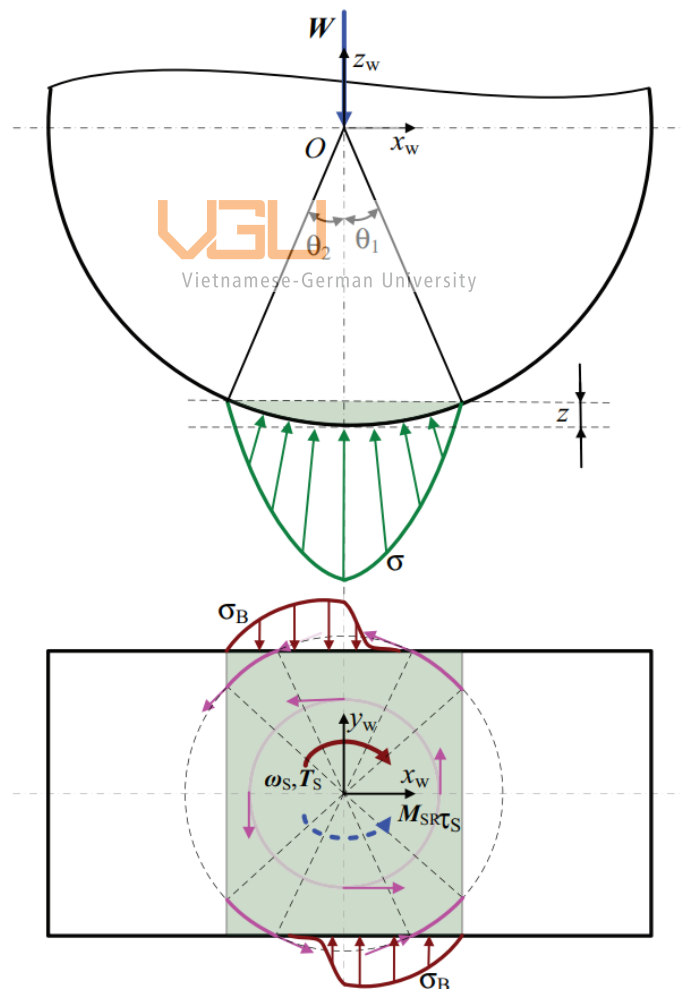


Figure 2.5 Stress distribution for in steering wheel [4]

Then the steering moment is caused by the shearing stress and the bulldoze stress, which are denoted by MSR1 and MSR2, respectively [4]

$$M_{SR} = M_{SR11} + M_{SR12} + M_{SR2}$$

Eqn 2.13

$$M_{SR11} = 2r \int_0^{\theta_1} \int_{-\frac{b}{2}}^{\frac{b}{2}} [c + \sigma(\theta) \tan \varphi] \left(1 - e^{-\frac{\sqrt{r^2 \theta + y_w^2} |\theta_s|}{K}} \right) \frac{r^2 \theta}{\sqrt{r^2 \theta + y_w^2}} dy_w d\theta$$

Eqn 2.14

$$M_{SR12} = 2r \int_0^{\theta_1} \int_{-\frac{b}{2}}^{\frac{b}{2}} [c + \sigma(\theta) \tan \varphi] \left(1 - e^{-\frac{\sqrt{r^2 \theta + y_w^2} |\theta_s|}{K}} \right) \frac{y_w^2}{\sqrt{r^2 \theta + y_w^2}} dy_w d\theta$$

Eqn 2.15

$$M_{SR2} = +2r^2 \cos \theta_1 \int_{\theta}^{\theta_1} \tan \theta [2ch_s(\theta) \cot X_c + \gamma h_s^2(\theta) X_c (1 + X_c \tan \varphi)] d\theta$$

Eqn 2.16

$$\sigma_1(\theta) = \left(\frac{k_c}{b} + k_\varphi \right) r^n (\cos \theta - \cos \theta_1)^n$$



Vietnamese-German University

$$\theta_1 = \arccos \left(1 - \frac{Z_r}{r} \right)$$

Eqn 2.17

Eqn 2.18

$$X_c = \frac{\pi}{4} - \frac{\varphi}{2}$$

Eqn 2.19

$$h_s(\theta) = \frac{r - \frac{r \cos \theta}{\cos \theta}}{\cos \theta}$$

Eqn 2.20

Symbol	Parameter and unit
M_{SR}	steering resistance moment acting on the wheel due to soil
M_{SR11}	the steering resistance moment caused by the lateral shearing stress component
M_{SR12}	the steering resistance moment caused by the longitudinal shearing stress component
M_{SR2}	steering moment is caused by bulldoze stress
θ_1	entrance angle of a wheel moving in the soil
b	wheel width
c	cohesion of the soil
$\sigma(\theta)$	normal stress
φ	internal friction angle of the soil
θ_S	steering angle of a wheel
K	shearing deformation modulus of the soil
γ	bulk density of the soil (N/m ³)
z_r	wheel sinkage

2.3.2 Ackermann steering geometry

Ackerman steering geometry is a steering arrangement commonly used in vehicles to ensure that the inner and outer front wheels follow different paths while turning. It is named after the German carriage builder Georg Lankensperger, who developed the concept in the late 18th century, and was later refined by the British engineer and inventor, Rudolph Ackerman. In Ackerman steering geometry, the steering pivot points for the front wheels are positioned in such a way that a line drawn through them intersects with the rear axle. When the wheels are turned, the inner wheel follows a tighter turning radius than the outer wheel, which prevents slipping or scuffing of the tires during turns. This geometry is designed to ensure that both wheels roll on their respective paths without any sideways sliding, providing better handling and stability during turns. Ackerman steering geometry is used in a variety of vehicles, including cars, trucks, and other four-wheeled vehicles. It is particularly important in vehicles with high-speed cornering, as it ensures that the wheels maintain proper contact with the road and reduces the risk of tire wear and skidding.

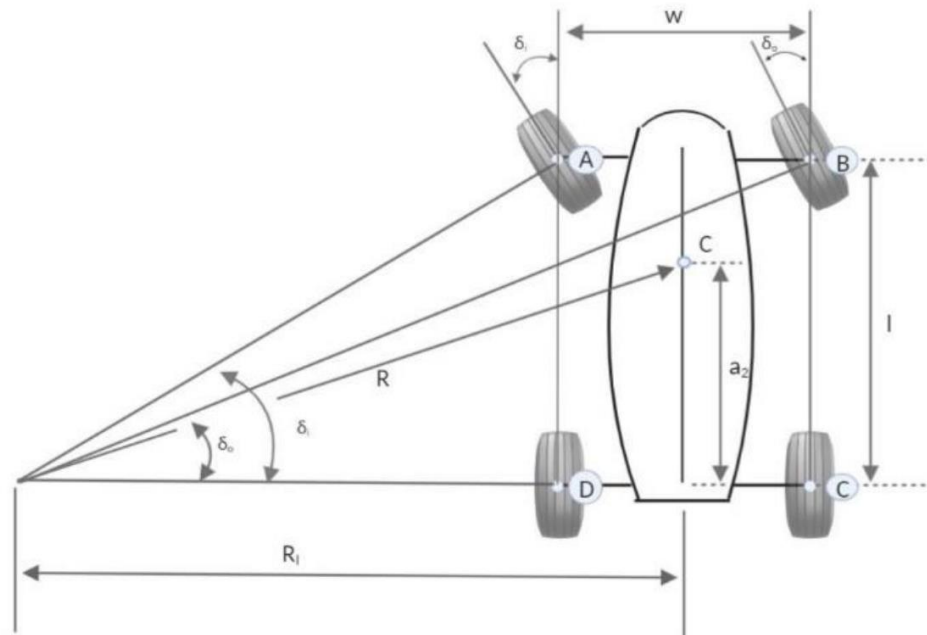


Figure 2.6 Vehicle turning in a Pro-Ackerman condition [5]

The Ackerman condition is a term used to describe a kinematic condition that occurs when a vehicle is moving at a very slow speed, and it allows for a turn to be made without any slippage between the inner and outer wheels. This condition is often expressed using follow equation [5].

$$\text{Cot}\delta_o - \text{Cot}\delta_i = \frac{w}{l}$$

Eqn 2.21

The steering angle of the inner and outer wheel is represented by δ_i and δ_o respectively, and these wheels are determined based on the turning center O [6]. The Center of Mass of the vehicle will rotate on a circle having a radius R. The value of R can be determined using follow equation.

$$R = \sqrt{a_2^2 + l^2 \text{Cot}^2 \delta}$$

Eqn 2.22

To determine the cot-average of the inner and outer steer angles, the cot values are computed using the given equation.

$$\text{Cot}\delta = \frac{\text{Cot}\delta_o + \text{Cot}\delta_i}{2}$$

The R is termed as the turning radius of the vehicle [10]. All these parameters are shown in Figure 2.6

3 Requirement determination

Requirement determination is the process of identifying, defining, and documenting the requirements that a project must meet in order to be considered a success. It involves gathering information about what the project is expected to deliver, what its goals and objectives are, and what the stakeholders expect from the final outcome. This information is then used to develop a clear and concise set of requirements that serves as the basis for the project's scope and provides a roadmap for the project team to follow.

Requirement determination is an essential step in the project planning process as it helps to ensure that the project is well-defined, well-planned, and aligned with the needs of the stakeholders. It is an iterative process that may involve several rounds of revisions and feedback, and it is critical to involve all relevant stakeholders in the process to ensure that all perspectives are considered.

3.1 Functional requirement

Functional requirements in product development refer to the specific capabilities, features, and performance characteristics that a product must have in order to meet the needs of its intended users. These requirements serve as a blueprint for the design and development of the product and help to ensure that the end result meets the desired specifications. Functional requirements typically include specifications for the product's functionality, performance, security, compatibility, reliability, and usability.

In terms of driving, the UGV should be capable of moving in a straight line above the vegetable plot. Steering is also an essential function, and the UGV should be designed to take up as little space as possible when moving between vegetable plots. The frame of the UGV should be adjustable in width and height, depending on the type of vegetable being cultivated, and should be able to follow the growth of the plants over time. Finally, the UGV should be practical, cost-effective, and easily assembled and disassembled. It should also be easy to operate and consist of popular components that can save money while still meeting the requirements for efficient and effective agricultural operations. Meeting these functional requirements is essential for the successful deployment of UGVs in agriculture, and can lead to significant improvements in productivity and efficiency.

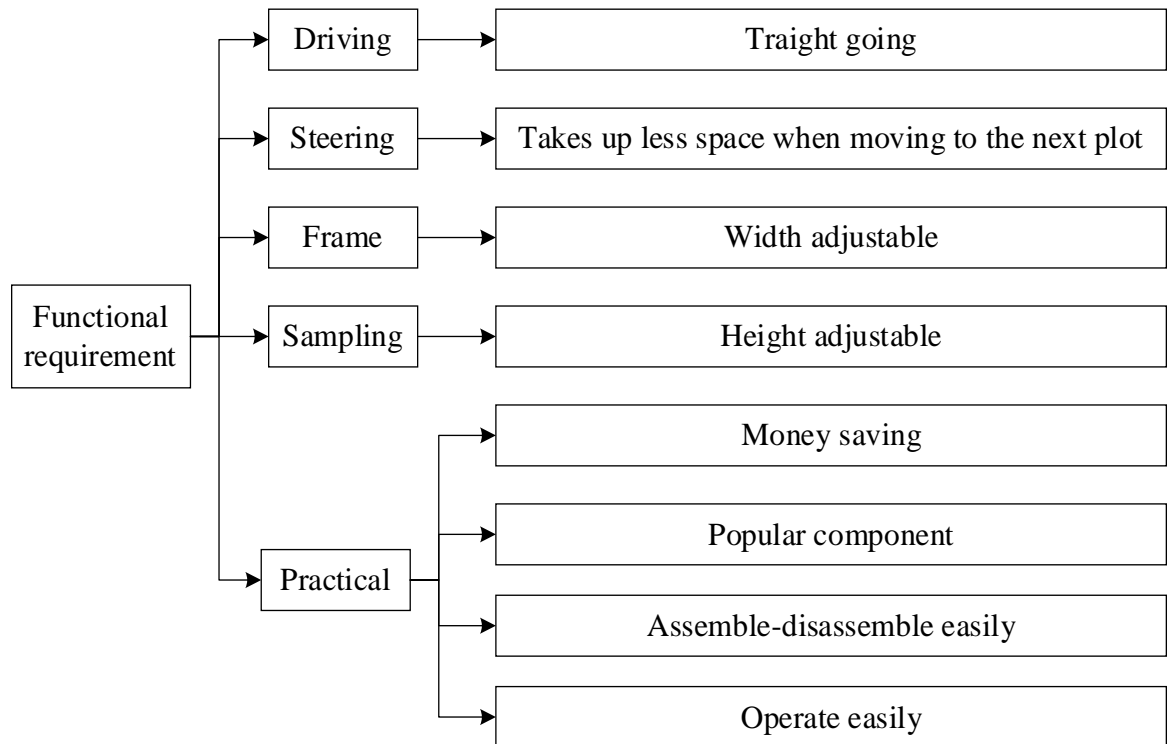


Figure 3.1 Functional requirement

3.2 Functional requirement evaluation

Vietnamese-German University

Table 3.1 Functional requirement evaluation

No.	Functional requirements	Rank
1	Straight going	7
2	Takes up less space when moving to the next plot	7
3	Money saving	5
4	Popular component	5
5	Assemble-disassemble easily	4
6	Operate easily	2

4 Development and selection

4.1 Concept

Table 4.1 Options table

Category	Choice		
Driving wheels number	2 wheels	4 wheels	Servo
Driving motor	DC	Stepper	
Driving mechanism	Direct	Gear + chain	
Steering mechanism	Skid steering	Actuator + arm	Wheels rotating

Since the selection of the motor type is largely influenced by the money-saving criterion, but the parameters of the required motor torque are not yet available, the motor type will be temporarily excluded from the options table. As a result, the evaluation of the functional requirements will exclude the money-saving criterion for the time being.

Table 4.2 Concept 1 – level basic

Category	Choice		
Driving wheels number	2 wheels	4 wheels	Wheels rotating
Driving mechanism	Direct	Gear + chain	
Steering mechanism	Skid steering	Actuator + arm	

Table 4.3 Concept 2 – level basic

Category	Choice		
Driving wheels number	2 wheels	4 wheels	Wheels rotating
Driving mechanism	Direct	Gear + chain	
Steering mechanism	Skid steering	Actuator + arm	

Table 4.4 Concept 3 – level intermediate

Category	Choice		
Driving wheels number	2 wheels	4 wheels	Wheels rotating
Driving mechanism	Direct	Gear + chain	
Steering mechanism	Skid steering	Actuator + arm	

Table 4.5 Concept 4 – level advance

Category	Choice		
Driving wheels number	2 wheels	4 wheels	
Driving mechanism	Direct	Gear + chain	
Steering mechanism	Skid steering	Actuator + arm	Wheels rotating

4.2 Concept evaluation

Table 4.6 Concept evaluation

Criteria		1	2	4	5	6	Sum
Weighting factor (%)		28	28	20	16	8	100
Concept 1	Core	7	4	3	4	1	19
	Weighted score (%)	196	112	60	64	8	440
Concept 2	Core	7	4	5	4	1	21
	Weighted score (%)	196	112	100	64	8	480
Concept 3	Core	6	4	4	3	2	19
	Weighted score (%)	168	112	80	48	16	424
Concept 4	Core	5	7	3	1	2	18
	Weighted score (%)	140	196	60	16	16	428

5 Implement of the chosen concept

5.1 Land properties

Farming land properties can vary widely depending on factors such as location, climate, soil type, and size. Some important properties of farming land include the type of soil and its fertility, the availability of water, and the overall climate of the region. Other factors that can impact the suitability of a piece of land for farming include the topography of the area, the presence of natural resources like forests or minerals, and the potential for erosion or flooding.



Figure 5.1 Vegetable plot
Vietnamese-German University

The typical type of agriculture soil for plating vegetable in Lam Dong is sandy loam, humus, basalt soil but sandy loam is the most popular one [7]. Because of the limitation of the topic, we do not perform experiments to determine properties of sandy loam, instead, we use the available data . From Appendix 1 we got value for n , k_c , k_ϕ , from [8], we got the estimation value for c , ϕ , γ and K is from [9],

Table 5.1 Sandy loam specification

Symbol	Parameter	Value
n	sinkage exponent of the soil	0.1
k_c	cohesive modulus of the soil	5.2 kN/m ⁿ⁺¹
k_ϕ	frictional modulus of the soil	321.11 kN/m ⁿ⁺²
c	cohesion of the soil	41 kN/m ²
ϕ	internal friction angle of the soil	35°
γ	bulk density of the soil	1.41 g/cm ³
K	shearing deformation modulus of the soil	10 mm

5.2 General design

Corresponding to the concept 2, we have a general design as follow.

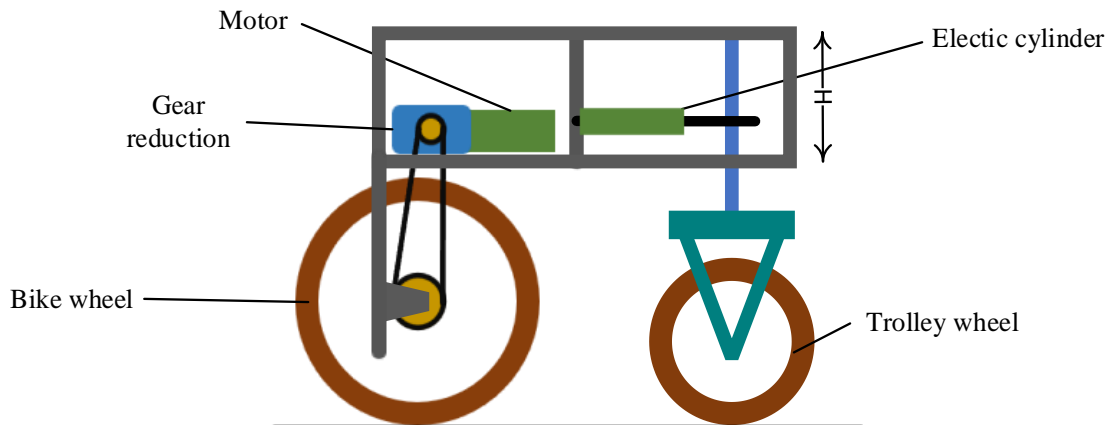


Figure 5.2 General design side view

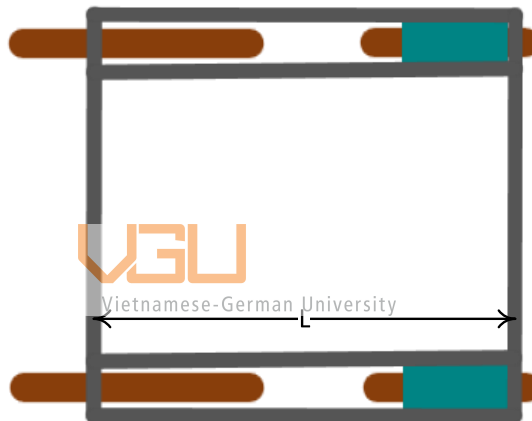


Figure 5.3 General design top view

Table 5.2 UGV specifications

Part	Symbol	Parameter	Value
UGV	m	mass	80 kg
	H	height	20 cm
	L	length	83 cm
bike wheel	D_1	diameter	40 cm
	r_1	radius	20 cm
	b_{i1}	width	4 cm
trolley wheel	p_{i1}	inflation pressure	30 psi
	D_2	diameter	20 cm
	r_2	radius	10 cm
	b_{i2}	width	4 cm

5.3 Driving kinetics

5.3.1 General

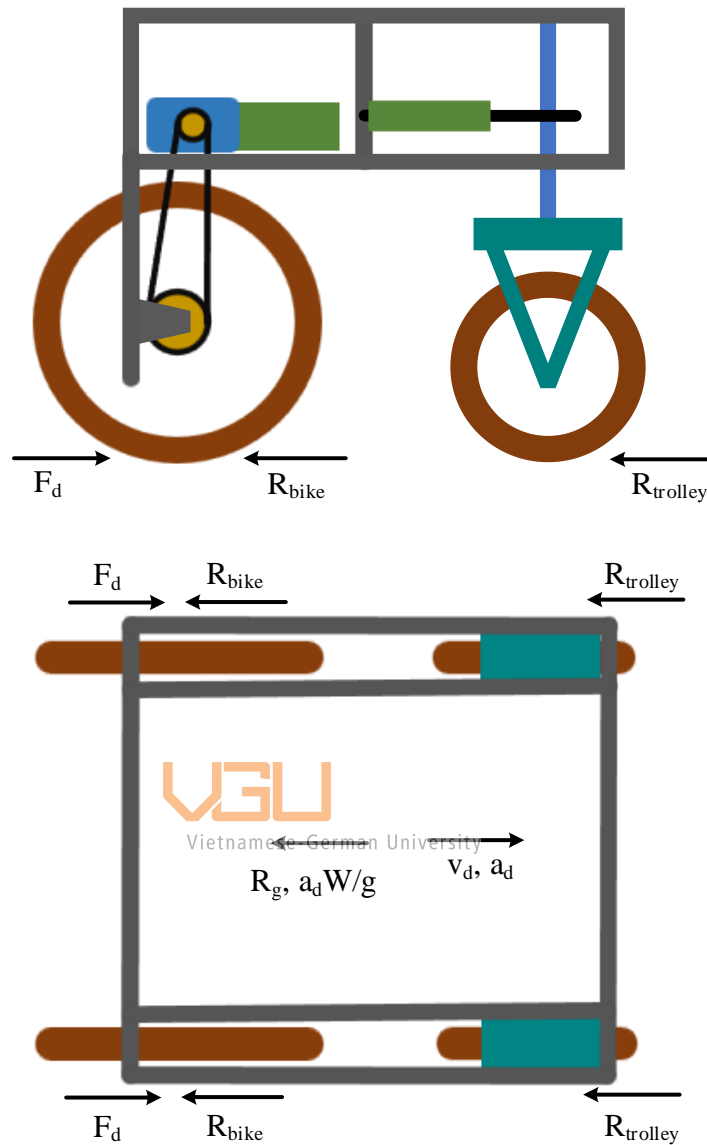


Figure 5.4 General forces

For an UGV with slow moving, there is no drag force R_a . The UGV is not pulling anything, so the draw bar F_d is zero. To find the motor torque require, we consider the situation of maximum thrust torque happen which is R_g have the negative sign. Using Eqn 2.1 we have the motion equation for the whole UGV.

$$\underline{F_d} = 2F_d = \frac{aW}{g} + 2R_{trolley} + 2R_{bike} + R_g$$

Eqn 5.1

The mass m of UGV is 80 kg. So, the total weight, and the weight apply on each wheel is

$$\underline{W} = mg = 800N$$

Eqn 5.2

$$W = \frac{\underline{W}}{4} = 200N$$

Eqn 5.3

We chose the slope angle is $\theta_s = 5^\circ$, it means that the UGV is working stable between $0 - 5^\circ$ and the maximum grade resistance is

$$R_g = \underline{W}\sin(\theta_s) = 70 N$$

Eqn 5.4

We want the operation acceleration is 0.5 m/s^2 . As a result, the inertia force is

$$\frac{aW}{g} = 16 N$$

Eqn 5.5

Symbol	Parameter	Value
\underline{W}	total weight	800 N
W	weight apply on each wheel	200 N
g	gravitational acceleration	9.81 m/s ²
θ_s	a slope at an angle to the horizontal which the vehicle operates on (degree)	5°
a	driving acceleration	0.5 m/s^2

5.3.2 Motion resistance

5.3.2.1 Bike wheel R_{bike}

First, we need to predict the operation mode using the method in 2.2.1.3 by comparing p_g and p_{gcr} . However, in this project p_g is not available due to lack of wheel specification. We know p_g is sum of p_c and p_i according to Eqn 2.5 but the p_c is relatively small to compare with the p_i , so we can only use p_i as an estimation of p_g .

$$p_{gcr} = \left[\frac{k_c}{b_{ti1}} + k_\phi \right]^{\frac{1}{2n+1}} \left[\frac{3W}{(3-n)b_{ti1}\sqrt{D_1}} \right]^{\frac{2n}{2n+1}} = 9.3 \text{ psi}$$

Eqn 5.6

Corresponding to wheel specification Table 5.2, using p_i as p_g we can see that $p_g > p_{gr}$. Therefore, the wheel will operate as a ridged wheel, and as a result the resistance is no resistance due to tire flexing.

Following the steps in 2.2.1.1 to determine the compaction resistance. First, we need to determine which is smaller between b_{ti} and l_t .

$$z_{r1} = \left(\frac{3W}{b_{ti1}(3-n) \left(\frac{k_c}{b_{ti1}} + k_\phi \right) \sqrt{D_1}} \right)^{\frac{2}{2n+1}} = 19 \text{ mm}$$

Eqn 5.7

$$l_{t1} = \sqrt{\left(\frac{D_1}{2}\right)^2 - \left(\frac{D_1}{2} - z_{r1}\right)^2} = 8.5 \text{ cm}$$

Eqn 5.8

Because l_{t1} is smaller than b_{ti1} so b_1 in the Eqn 5.8 is l_{t1}

$$R_{bike} = \frac{1}{(3-n)^{\frac{2n+2}{2n+1}}(n+1)b_{ti1}^{\frac{1}{2n+1}} \left(\frac{k_c}{b_1} + k_\phi \right)^{\frac{1}{2n+1}} \left(\frac{3W}{\sqrt{D_1}} \right)^{\frac{2n+2}{2n+1}}} = 85 \text{ N}$$

Eqn 5.9

5.3.2.2 Trolley wheel $T_{trolley}$



Vietnamese-German University

The type of front wheel is ridged wheel, so there is no resistance due to flexing. Follow the same step of the front wheel.

$$z_{r2} = \left(\frac{3W}{b_{ti2}(3-n) \left(\frac{k_c}{b_2} + k_\phi \right) \sqrt{D_2}} \right)^{\frac{2}{2n+1}} = 29 \text{ mm}$$

Eqn 5.10

$$l_{t2} = \sqrt{\left(\frac{D_2}{2}\right)^2 - \left(\frac{D_2}{2} - z_{r2}\right)^2} = 7 \text{ cm}$$

Eqn 5.11

Because l_{t2} is smaller than b_2 so b in the Eqn 5.11 is l_{t2} .

$$R_{trolley} = \frac{1}{(3-n)^{\frac{2n+2}{2n+1}}(n+1)b_{ti2}^{\frac{1}{2n+1}} \left(\frac{k_c}{b_2} + k_\phi \right)^{\frac{1}{2n+1}} \left(\frac{3W}{\sqrt{D_2}} \right)^{\frac{2n+2}{2n+1}}} = 150 \text{ N}$$

Eqn 5.12


5.4 Steering kinetics

5.4.1 Steering geometry

5.4.1.1 Steering radius estimation

The design of the UGV's steering mechanism is an important aspect of the overall system. To simplify the design and reduce the complexity of the system, we decided to use the parallel steering mechanism instead of the normal Ackermann steering mechanism. With this mechanism, the outer and inner steering angles of the two front wheels are equal, which makes it easier to control and adjust the steering system. Despite using the parallel steering mechanism, we still used the Ackermann formula to estimate our turning radius, as it is a widely accepted and reliable method. To further improve our estimation, experiments will be conducted to test the UGV's turning radius in various conditions. By doing so, we can ensure that our UGV is able to navigate through tight turns and confined spaces with precision and accuracy.

The minimum turning radius of the UGV was estimated using the Ackermann formula (Eqn 2.2), taking into account the maximum steering angle of 25 degrees and assuming the center of mass to be located at the center of the vehicle ($a_2 = 0.83/2 = 0.415$ m). The steering radius (with respect to the center) is calculated by follow equation.



$$R = \sqrt{a_2^2 + l^2 \cot^2 \delta} = 1.83 \text{ m}$$

Eqn 5.13

Follow Figure 2.6, we calculate R_i by follow equation

$$R_i = \sqrt{R^2 - a_2^2} = 1.78 \text{ m}$$

Eqn 5.14

The steering radius (with respect to the outer wheel) is calculated by the follow equation

$$\bar{R} = R_i + \frac{B}{2} = 2.22 \text{ m}$$

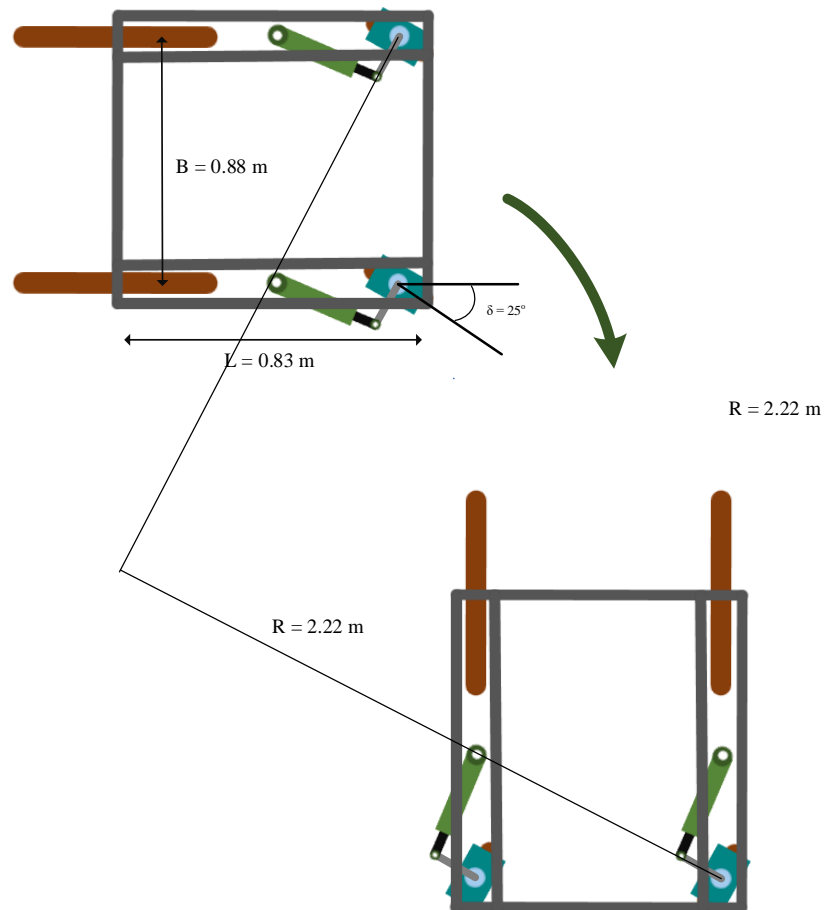



 Figure 5.5 Theoretical steering model
Vietnamese-German University

5.4.2 Steering resistance moment

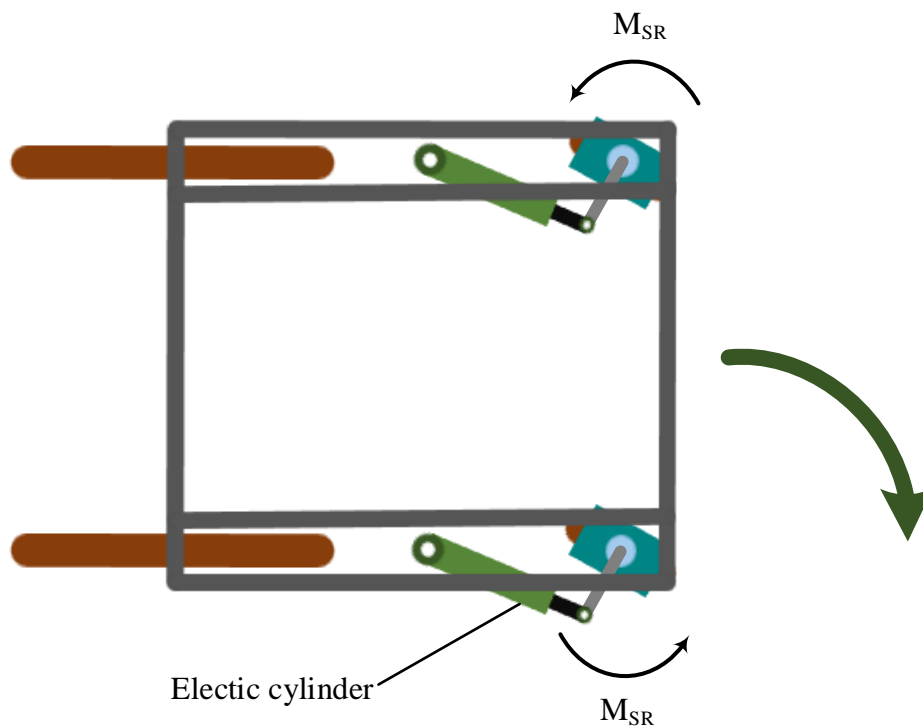


Figure 5.6 General steering design

The steering resistance moment is only appeared in trolley wheel, so we assume some symbol below as $r = r_2$, $b = b_{ti2}$, $z_r = z_{r2}$. We want the steering angle θ_s in this case is 30° .

$$X_c = \frac{\pi}{4} - \frac{\varphi}{2} = 27.5^\circ$$

Eqn 5.15

$$\theta_1 = \arccos\left(1 - \frac{z_r}{r}\right) = 28.6^\circ$$

Eqn 5.16

$$M_{SR11} = 2r \int_0^{\theta_1} \int_{-\frac{b}{2}}^{\frac{b}{2}} [c + \sigma(\theta)\tan\varphi] \left(1 - e^{-\frac{\sqrt{r^2\theta + y_w^2} |\theta_s|}{K}}\right) \frac{r^2\theta}{\sqrt{r^2\theta + y_w^2}} dy_w d\theta = 6.2 \text{ Nm}$$

Eqn 5.17

$$M_{SR12} = 2r \int_0^{\theta_1} \int_{-\frac{b}{2}}^{\frac{b}{2}} [c + \sigma(\theta)\tan\varphi] \left(1 - e^{-\frac{\sqrt{r^2\theta + y_w^2} |\theta_s|}{K}}\right) \frac{y_w^2}{\sqrt{r^2\theta + y_w^2}} dy_w d\theta = 1.3 \text{ Nm}$$

Eqn 5.18

$$M_{SR2} = 2r^2 \cos\theta_1 \int_{\theta}^{\theta_1} \tan\theta [2ch_s(\theta)\cot X_c + \gamma h_s^2(\theta)X_c(1 + \cot X_c \tan\varphi)] d\theta = 1.4 \times 10^{-16} \text{ Nm}$$



Vietnamese-German University

Eqn 5.19

$$\sigma(\theta) = \left(\frac{k_c}{b} + k_\varphi\right) r^n (\cos\theta - \cos\theta_1)^n$$

Eqn 5.20

$$h_s(\theta) = \frac{r - \frac{rcos\theta}{cos\theta}}{cos\theta}$$

Eqn 5.21

$$M_{SR} = M_{SR11} + M_{SR12} + M_{SR2} = 7.9 \text{ Nm}$$

Eqn 5.22

6 Manufacturing

6.1 Motor and transmission

6.1.1 Required motor power

From equation Eqn 5.1 we got

$$\underline{F_d} = \frac{aW}{g} + 2R_{trolley} + 2R_{bike} + R_g = 253 \text{ N}$$

Eqn 6.1

$$F_d = \frac{F_d}{2} = 127 \text{ N}$$

Eqn 6.2

Symbol	Parameter	Formula	Value
η_t	gear reduction efficiency	n/a	90 %
M_w	required moment at each wheel	$M_w = \frac{F_d r_1}{\eta_t}$	30 Nm
v_d	driving velocity	n/a	1-3 m/s
ω_w	angular velocity of wheel	$\omega_w = \frac{v}{r_1}$	5-15 π rad/s
n_w	speed of wheel	$n_w = \frac{60\omega_w}{2\pi}$	48-150 RPM
P_m	required motor power	$P_m = \frac{M_w n_w}{9.5}$	155-460 W

To simplify the process of choosing a motor later on, we have decided to set the driving velocity to a range of 1-3 m/s. By establishing this range, we can narrow down the list of motors we need to consider and focus on those that are suitable for our required driving velocity. This will save us time and effort in the selection process, as we won't have to sift through a large number of motors that are not compatible with our desired velocity range. Additionally, by setting a specific range, we can ensure that the selected motor is capable of providing the necessary power and speed to maintain the desired velocity without any issues. This approach will help us make an informed decision and choose the most suitable motor for our needs.

6.1.2 Motor choosing

There are many different types of electric motors, each with their own characteristics and applications. Here are some of the most common types:

- DC motors: These motors use direct current (DC) to power the rotor, and can provide precise speed and torque control.
- Stepper motors: These motors move in small, precise steps, and are commonly used in printers, robotics, and other applications that require precise control.
- Servo motors: These motors are used in applications that require precise control of position, speed, or torque, and often incorporate feedback mechanisms to ensure accurate control.

Here are some of the key differences between these motor types:

Table 6.1 Motor type comparison

Aspects	DC motor	Stepper	Servo
Control	basic speed control	move in small, precise steps	precise control of position, speed, or torque
Feedback	do not have feedback	not require feedback	use feedback mechanisms to ensure accurate control
Torque	can provide high starting torque	can provide high holding torque at low speeds	can provide high torque over a wide range of speeds
Efficiency	relatively inefficient at low speeds	inefficient at high speeds	more efficient across a wide range of speeds
Cost	most affordable option	more expensive	more expensive
30Nm motor price	~ 2,000,000 VND	~ 7,500,000 VND	~ 8,000,000 VND

While stepper and servo motors offer precise control in robotics, their high cost can be a limiting factor. For this thesis, we will focus on using the basic speed control of a DC motor to complete the project. While this may not offer the same level of precision as a stepper or servo, it will be sufficient for the scope of this project. Additionally, other improvements can be made in the future to further enhance the control and precision of the system. For now, we will focus on completing the project using the most cost-effective means available.

Symbol	Parameter	Formula	200W motor	300W motor
P_m	motor power	n/a	200 W	300 W
n_m	operation motor speed	n/a	2350 RPM	2350 RPM
μ	safety coefficient	n/a	0.7	0.7
n_w	speed of wheel	$\frac{P_m 9550}{1000 M_w} \times 0.7$	44 RPM	66 RPM
ω_w	angular velocity of wheel	$\frac{n_w 2\pi}{60}$	4.6 π rad/s	6.9 π rad/s
v	UGV speed	$\omega_w \times r_1$	0.92 m/s	1.38 m/s
t_o	operation time	n/a	0.6 h	0.5 h (*)
m	price	n/a	2,000,000 VND	2,500,000 VND

(*) The operation time is calculated by the following step

Used battery: 2 x (12V, 12Ah)

Battery capacity: 12V x 12Ah x 2 = 288Wh

Suppose the motor operating with 80% power in average

Electricity consumed of motor in an hour: 300W x 2 x 1h x 80% = 480W

Electricity consumed of electric cylinder in an hour: 12W x 2 x 1h = 24Wh

Electricity consumed of other components: 20Wh (assume)

Operation time: 288 / (480 + 24 + 20) = 0.55h

After analyzing the table, we have concluded that the best option for our needs is the 300W motor. The main reason behind our decision is that it provides a higher operation speed compared to the 200W motor. Additionally, we found that the 300W motor is not significantly more expensive than the 200W motor, which makes it a cost-effective option. Furthermore, we noticed that choosing the 300W motor does not have a significant impact on the operation time. Overall, the 300W motor is the best choice for our needs due to its speed, cost-effectiveness, and minimal impact on the operation time.

Motor DC - điện 1 chiều 12v hoặc 24v
Nguồn điện 12v tốc độ: motor ~1100 vòng phút
Nguồn điện 24v tốc độ: motor ~2350 vòng phút

ISO 9001

① Motor DC mã 5
 195
 Minhmotor
 Đường kính trục 11
 Rãnh cavet 4

②

③ Hộp số GN 5
 102.5
 Minhmotor
 73.5
 90

Với motor giảm tốc DC, hãy lựa chọn tốc độ như bảng sau:

④ Đường kính trục 15mm
 272
 Minhmotor
 300w
 Gồm 2 bộ phận như ảnh bên phải.

Thứ Tự	Tỉ số truyền, Ratio i	Điện 12V, motor 1 chiều		Điện 24V, motor 1 chiều	
		Tốc độ trực ra, 1100/ i	Tốc độ trực ra, 2350/ i	Tốc độ trực ra, 1100/ i	Tốc độ trực ra, 2350/ i
1	5	220	470		
2	10	110	235		
3	15	73	157		
4	20	55	118		
5	25	44	94		
6	30	37	78		
7	40	28	59		
8	50	22	47		
9	60	18	39		
10	80	14	29		
11	100	11	24		
12	200	6	12		

* Motor, hộp giảm tốc giảm tốc xuất khẩu **Châu Âu**.
 * Bánh răng - nhôm làm từ thép chống rỉ, **siêu bền**.
 * Dây truyền robot hóa tự động CNC

Figure 6.1 300W motor

Based on the analysis of the requirements and specifications for the UGV, a 300W DC motor with a 24V DC supply and an operation speed of 2350 RPM has been chosen as the optimal solution. This type of motor is commonly used in automation and robotics applications, providing a balance between power and efficiency. In addition, this type of motor usually comes with a reduction gearbox that can further increase torque and decrease speed for more precise control. The specific reduction ratio for the motor will be calculated in the next section of the thesis to ensure optimal performance for the UGV.

6.1.3 Transmission system

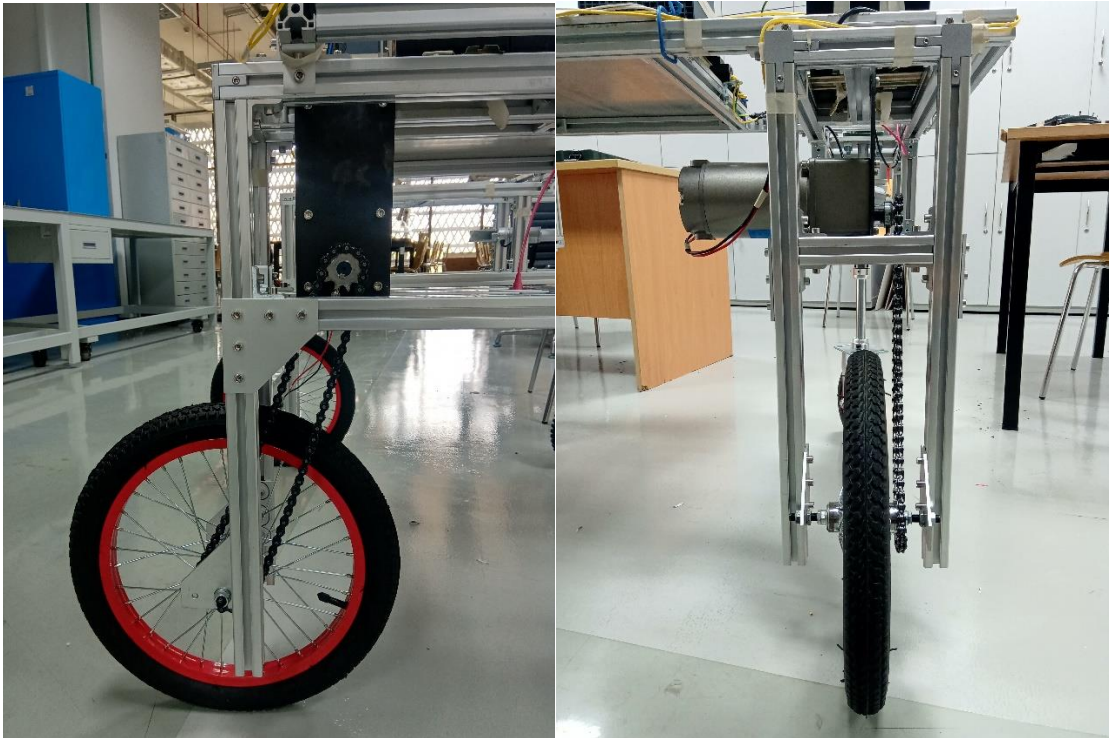


Figure 6.2 Transmission system side view (left) and back view (right)

A reduction gearbox is a mechanical device that is used to reduce the speed of a DC motor and increase its torque. The gearbox consists of a set of gears that mesh together to transmit power from the motor to an output shaft. The gear ratio is what determines the speed and torque of the output shaft. The reduction gearbox is commonly used in applications where the speed of the motor needs to be reduced, while the torque needs to be increased (the ratios can be found in the figure above). By using a reduction gearbox, the DC motor can be optimized for the specific requirements of the application, resulting in greater efficiency, performance, and longevity of the motor.

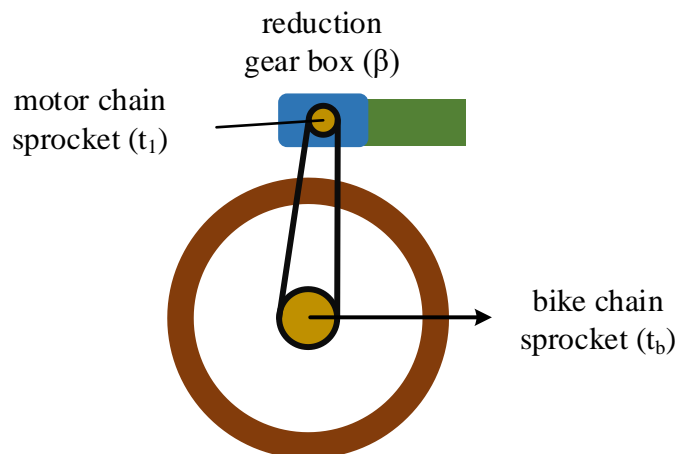


Figure 6.3 Transmission diagram

A chain sprocket is a toothed wheel that meshes with a chain, transmitting power and motion between the rotating shaft of a machine and a chain-driven component, such as a wheel or another sprocket. It has some basic specifications:

1. Pitch diameter: the diameter of the circle that intersects with the center of the sprocket teeth
2. Number of teeth: the number of teeth on the sprocket that mesh with the chain
3. Pitch: the distance between the center of two adjacent chain pins
4. Bore diameter: the diameter of the hole in the center of the sprocket where it attaches to the shaft
5. Hub diameter: the diameter of the flange that extends out from the sprocket and provides support for the chain

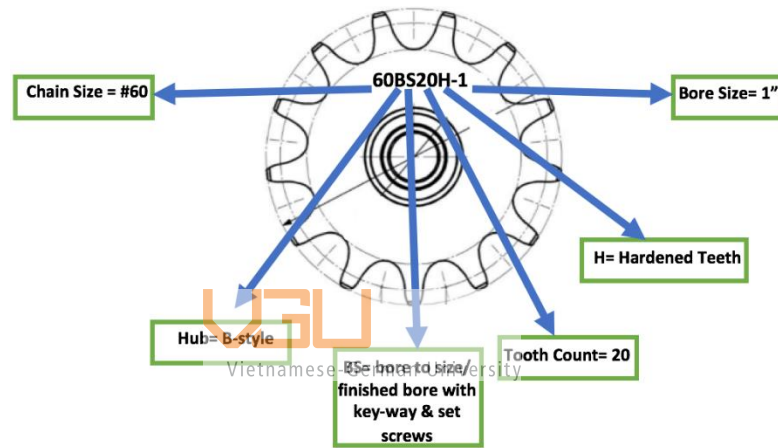


Figure 6.4 Sprocket size nomenclature

Figure 6.5 is the chain sprocket RS40-10TB that I use for this project. It has specifications as follows:

1. RS40: the name of the corresponding sprocket gear associated with the chain 40 and has a few basic parameters as follows
 - P (chain pitch, pitch): 12.7mm
 - B (thickness of teeth): 7.2mm.
 - Dr (roller diameter): 7.95mm
2. 10: Number of teeth
3. TB: The type has a hunchback on one side.
4. Material: C45



Figure 6.5 Chain sprocket RS40-10TB

The machine technique of turning was employed to reduce the teeth thickness of the chain sprocket from 7.2mm to 2.8mm. This method involves the use of a lathe machine to remove material from the sprocket teeth. The process was carefully controlled to ensure that the final tooth profile is accurate and precise, as any errors can result in poor performance or premature wear of the chain. By decreasing the teeth thickness, the sprocket can engage the chain more tightly, providing better power transmission and reducing the risk of the chain slipping off the sprocket. The final product of this machining process is a high-quality sprocket with teeth that are precisely machined to the desired thickness.



Vietnamese-German University

Symbol	Parameter	Formula	Value
t_b	bike chain sprocket teeth number	n/a	17
t_m	motor chain sprocket teeth number	n/a	10
ω_w	reduction ratio	$\beta = \frac{n_m}{n_w} \times \frac{t_m}{t_b}$	20

6.2 Steering mechanism

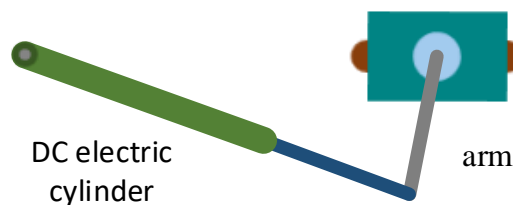


Figure 6.6 General design

The reasons why I chose an electric cylinder for my UGV steering mechanism are simple. Firstly, electric cylinders are a popular component that can be easily found on the market. They are a well-established technology and come in various shapes and sizes to fit different

applications. Secondly, electric cylinders are easy to assemble and require minimal maintenance. With their plug-and-play design, it is relatively straightforward to integrate them into a complex system without requiring extensive technical expertise.

6.2.1 DC electric cylinder

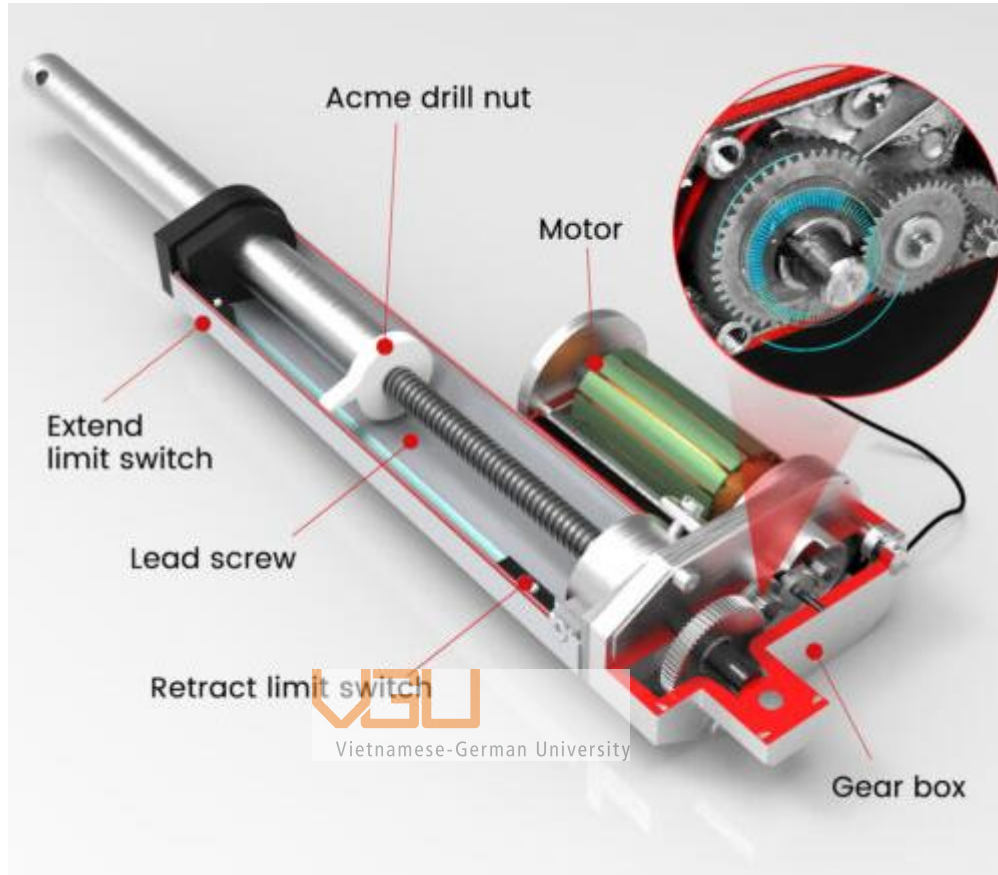


Figure 6.7 A 12V DC electric cylinder

A DC electric cylinder is an electromechanical device that converts electrical energy into linear motion. A DC electric cylinder typically consists of several key components that work together to convert electrical energy into linear motion. The basic mechanism of a DC electric cylinder involves a motor that drives a lead screw or belt, which in turn moves the piston or rod in the cylinder.

The motor is usually a DC motor, although some electric cylinders may use other types of motors as well. The motor provides the rotational force that drives the lead screw or belt. The lead screw or belt is connected to the motor shaft and converts the rotational motion of the motor into linear motion. The lead screw or belt is typically connected to a nut or pulley that is attached to the piston or rod.

The piston or rod moves in and out of the cylinder body to perform work. The linear motion is achieved through the interaction of the lead screw or belt with the nut or pulley. As the lead

screw or belt rotates, the nut or pulley moves, causing the piston or rod to move in the desired direction.

6.2.2 DC electric cylinder requirement

The following steps are taken to define the requirement of the electric cylinder.

We want the maximum steering angle is $\theta_s = 60^\circ$

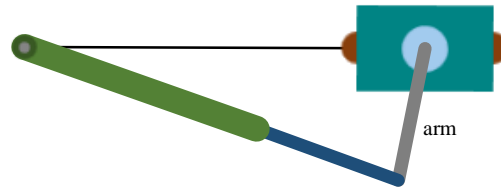
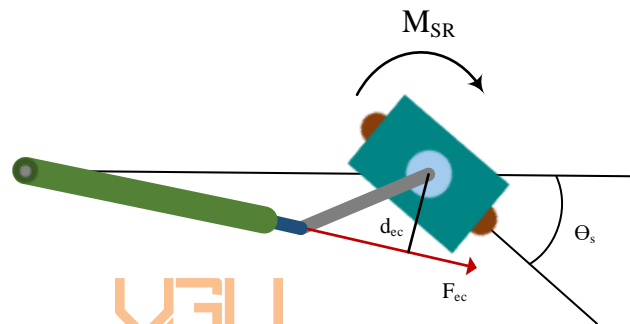


Figure 6.8 Straight going.



VGU

Vietnamese-German University

Figure 6.9 Turning right

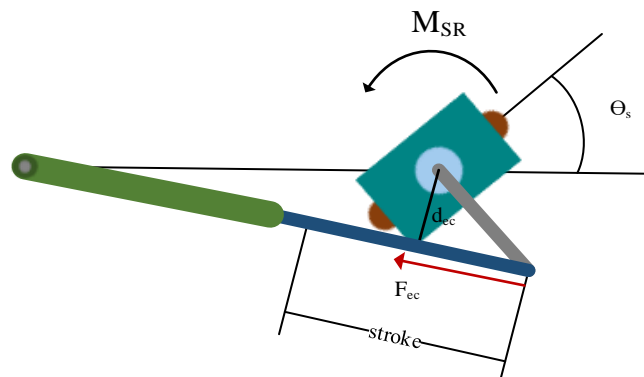


Figure 6.10 Turning left

The power of the electric cylinder must be large enough to cover the situation of Figure 6.9 and Figure 6.10, which is

$$F_{ec}d_{ec} > M_{SR} = 7.9 \text{ Nm}$$

Eqn 6.3

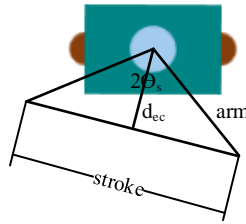


Figure 6.11 Electric cylinder stroke

We also have the condition of electric cylinder stroke from Figure 6.11

$$d_{ec} = \frac{1}{2} \text{stroke} \times \cot(\theta_s)$$

Eqn 6.4

Eqn 5.22 become

$$F_{ec} \times \frac{1}{2} \text{stroke} \times \cot(\theta_s) > M_{SR} = 7.9 \text{ Nm}$$

Eqn 6.5

For easily manufacturing, we choose the stroke of 100 mm, from Eqn 6.4 we got

$$F_{ec} > \frac{M_{SR}}{\text{stroke} \times \cot(\theta_s)} = 273 \text{ N}$$

Eqn 6.6

From geometry we got

$$\text{stroke} = 2\text{arm}^2 - 2\text{arm}^2 \cos \cos(2\theta_s) \rightarrow \text{arm} = \frac{\text{stroke}}{\sqrt{2(1 - \cos \cos(2\theta_s))}} = 5.8 \text{ cm}$$

Eqn 6.7

Symbol	Parameter and unit
θ_s	maximum steering angle
F_{ec}	force needed from electric cylinder
d_{ec}	lever arm

6.3 Control system

6.3.1 Control system overview

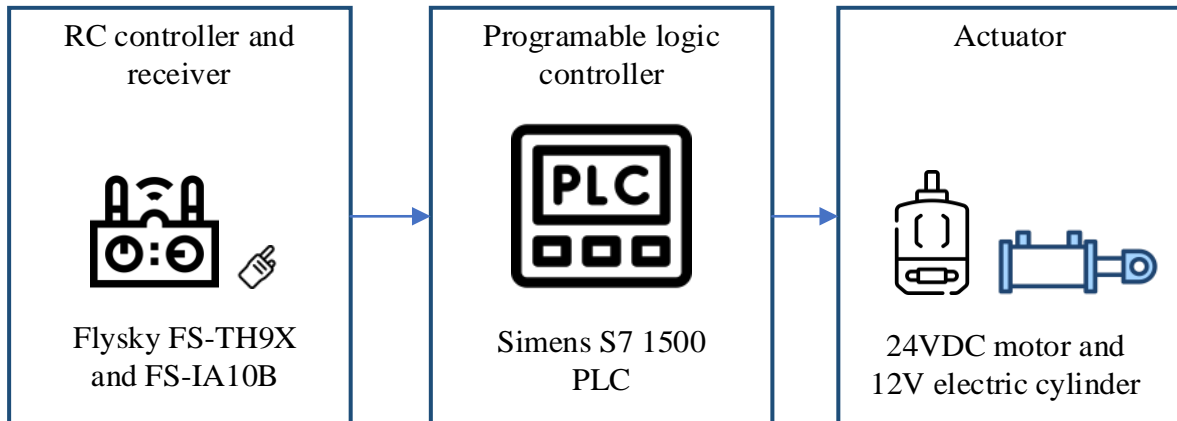


Figure 6.12 Control system overview

Due to the limitations of the project, we will be using a manual method for controlling the UGV. The idea is to use a PLC (S7-1500) with digital inputs and outputs. A RC controller and a receiver is used for the inputting signal. Later improvements related to automation will take place in the future.



Figure 6.13 Siemens S7-1500 PLC

The Siemens S7-1500 is a programmable logic controller (PLC) designed for use in industrial automation applications. It is part of Siemens' SIMATIC S7-1500 series and is known for its high processing speed, flexible communication options, and powerful functionality. The S7-1500 PLC can be used to control a wide range of industrial processes, including manufacturing, material handling, and building automation. It features multiple input and output modules, as well as a variety of communication options, including Ethernet and PROFINET, which allow it to connect with a range of devices and systems. Additionally, the S7-1500 PLC includes advanced features such as motion control, safety functionality, and energy management, making it well-suited for demanding industrial applications.

The Siemens S7-1500 programmable logic controller (PLC) is also ideal for controlling unmanned ground vehicles (UGVs). The PLC's high processing speed, flexible communication options, and powerful functionality make it well-suited for use in UGV control systems. It can be used to monitor and control various aspects of UGV operation, such as movement, sensor data acquisition, and navigation. For instance, the S7-1500 PLC can control the drive motors of a UGV, allowing it to move in a specific direction and at a specified speed. Furthermore, it can monitor the UGV's sensors and process the data they generate to provide information on the environment surrounding the UGV.

6.3.2 Input components

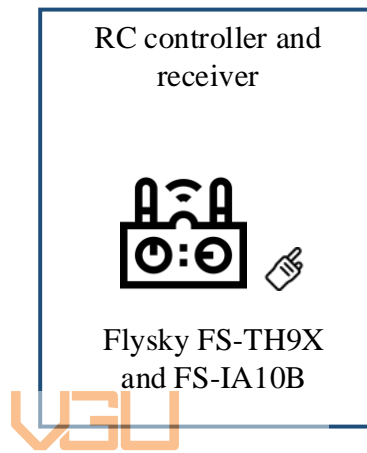


Figure 6.14 Input module

The UGV is manually controlled, and the input to the PLC is received via an RC transmitter and a receiver. I use the FlySky FS-TH9X for transmitting the signal, and the FS-iA10B for receiving the signal, which is then input to the PLC.



Figure 6.15 FlySky FS-TH9X

The FlySky FS-TH9X is a remote control transmitter used for controlling remote control vehicles such as drones, planes, and cars. It operates on the 2.4GHz frequency band and features

a large, backlit LCD screen for easy visibility in all lighting conditions. The FS-TH9X is equipped with a variety of channels, allowing for precise control of multiple functions on the remote control vehicle. Additionally, it features a smooth, dual-rate system for precise control of the vehicle's movements. Overall, the FlySky FS-TH9X is a popular and reliable remote control transmitter used by hobbyists and professionals alike for controlling their remote control vehicles.



Figure 6.16 Receiver FS-iA10B

The FS-iA10B is a 10-channel receiver that uses the AFHDS 2A protocol and operates on the 2.4GHz frequency. It is compatible with a range of FlySky transmitters, including the FS-i6, FS-i6S, FS-i6X, FS-i8, FS-i10, and FS-iT4S. The receiver features dual antennas, failsafe protection, and a range of up to 1.5km. It is commonly used in radio-controlled vehicles and other remote control applications.

6.3.3 PLC wiring

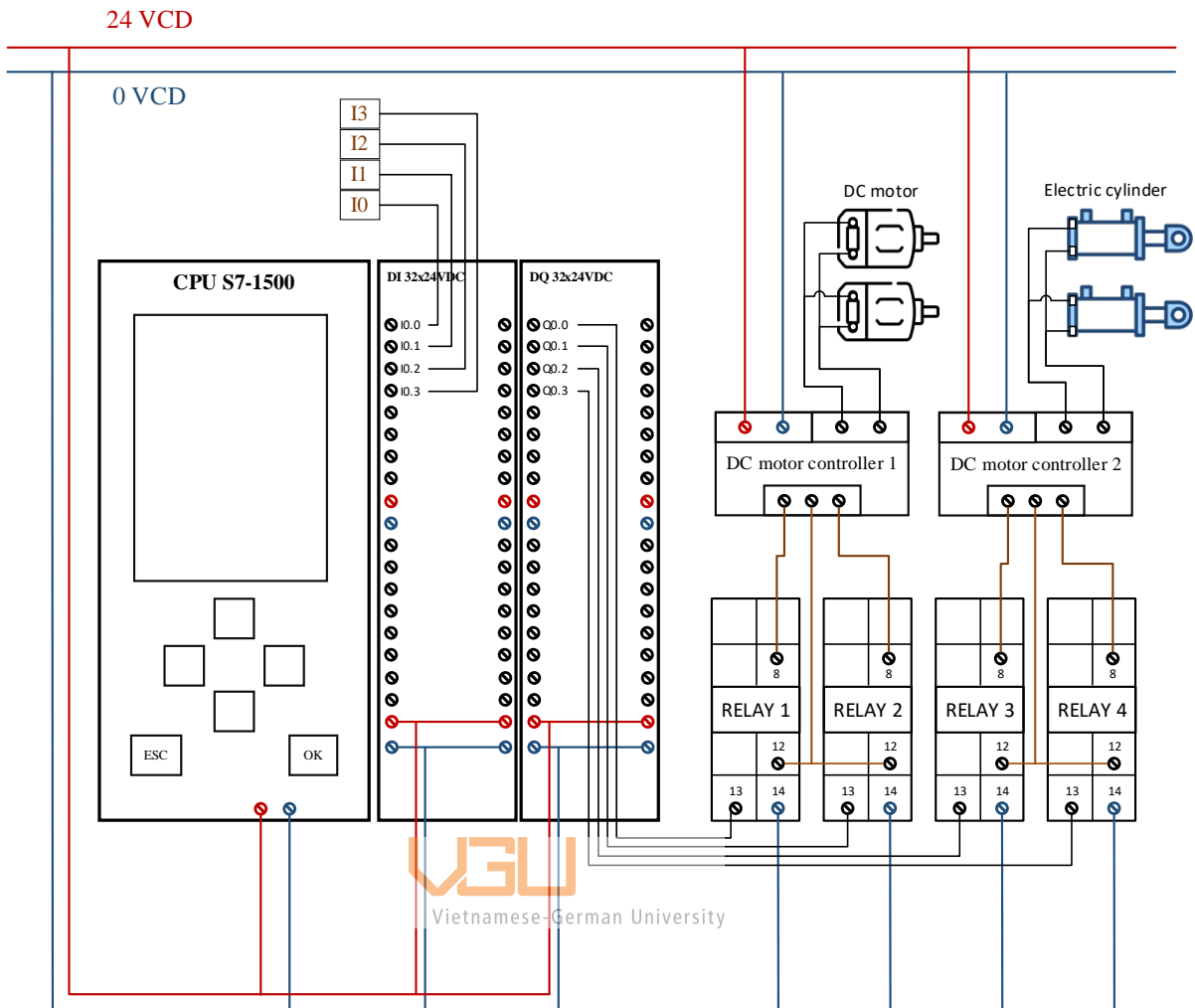


Figure 6.17 PLC wiring

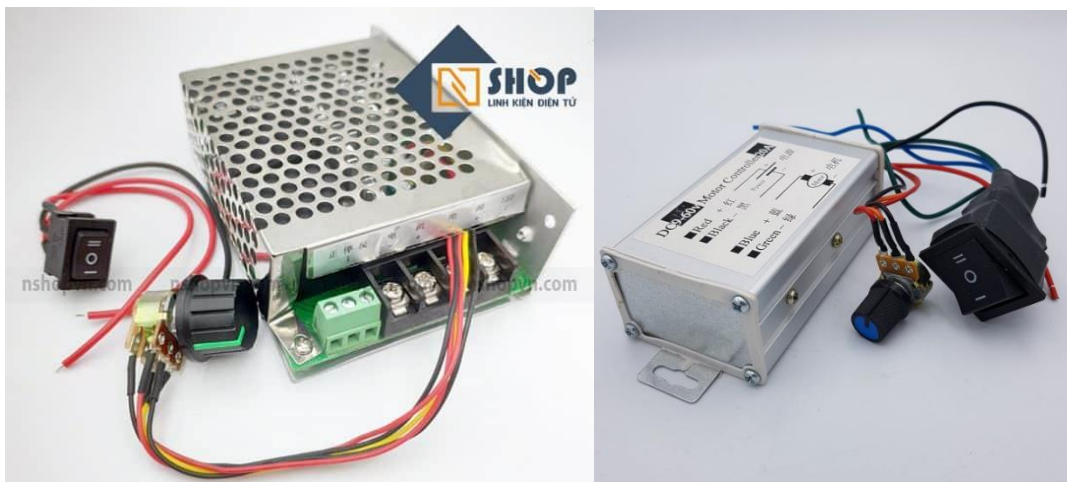


Figure 6.18 DC motor controller 1 (left) and 2 (right)

DC motor controllers (DMC) are essential electrical components that are responsible for controlling the speed and motion direction of the motor. Both DCM 1 and DCM 2 operate on a 24V DC power supply, and DCM 1 can handle a maximum current of 40A, while DCM 2 can

handle a maximum current of 20A. These motor controllers come equipped with a rheostat, which allows for the motor's speed to be controlled by increasing or decreasing the voltage supply to the motor. DCM 1 is used to control two DC motors, while DCM 2 is used to control two DC electric cylinders. They both have a switch to reverse the motion of the motor or electric cylinder, allowing for greater control over the UGV's movements.

6.4 Components list

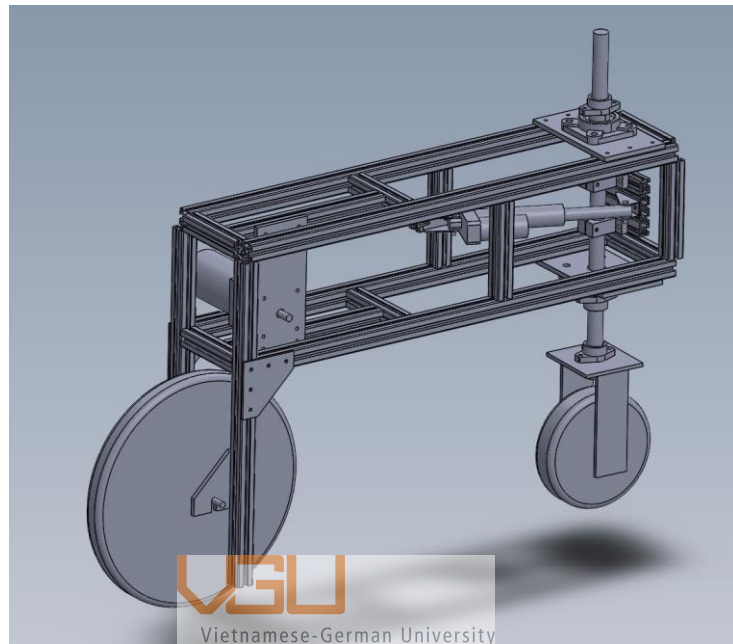










Figure 6.19 Design overview



Figure 6.20 Prototype

Components	Specification	Picture
Motor + reduction gearbox	24V, 300W, 2350 RPM, reduction ratio 20	
Motor chain sprocket	12 teeth	
Bike chain sprocket	17 teeth	
Chain	70 cm	
Bike wheel	16 inches	

Electric cylinder	12 V, stroke 100 mm, 900 N, 10 mm/s	
Cylinder bracket	N/A	
Trolley wheel	300kg capacity stainless steel  Vietnamese-German University	
Trolley wheel shaft	Φ 25	
SHF25	Φ 25	
SK25	Φ 25	

UCF205	Φ 25	
3030 L bracket	N/A	
90 degrees bracket	N/A	
3030 shaped aluminums	N/A	



Vietnamese-German University

6.5 Experiment

6.5.1 Driving experiment



Figure 6.21 Straight driving testing

The driving experiment was conducted to verify that the UGV can move along a straight line as expected. The experiment was performed as shown in Figure 3. To ensure accuracy, the measurements were taken three times. The results showed that the UGV was able to move straight without deviating from the intended path. Furthermore, to provide visual evidence of the UGV's performance, a video recording of the experiment was taken. The experiment results confirmed the effectiveness of the UGV's driving system in maintaining a straight-line trajectory.

6.5.2 Steering experiment

We conducted an experiment to measure the steering radius of our UGV. We found that our UGV was turning stably with a maximum steering angle of less than 24 degrees. Therefore, we used 24 degrees as the maximum steering angle for the experiment. We took several

measurements to ensure accuracy and recorded the results. The data obtained from this experiment will be useful in further improving the design of our UGV's steering system.

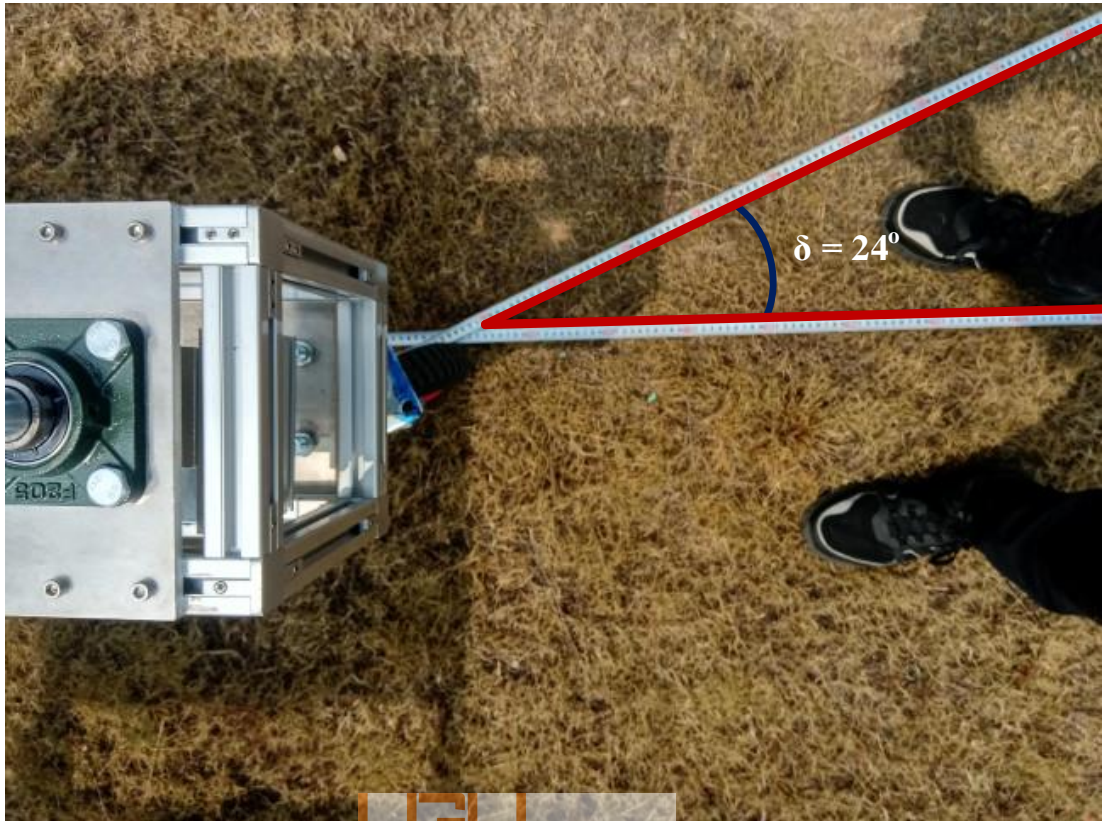


Figure 6.22 Experiment steering angle



Figure 6.23 1st steering experiment

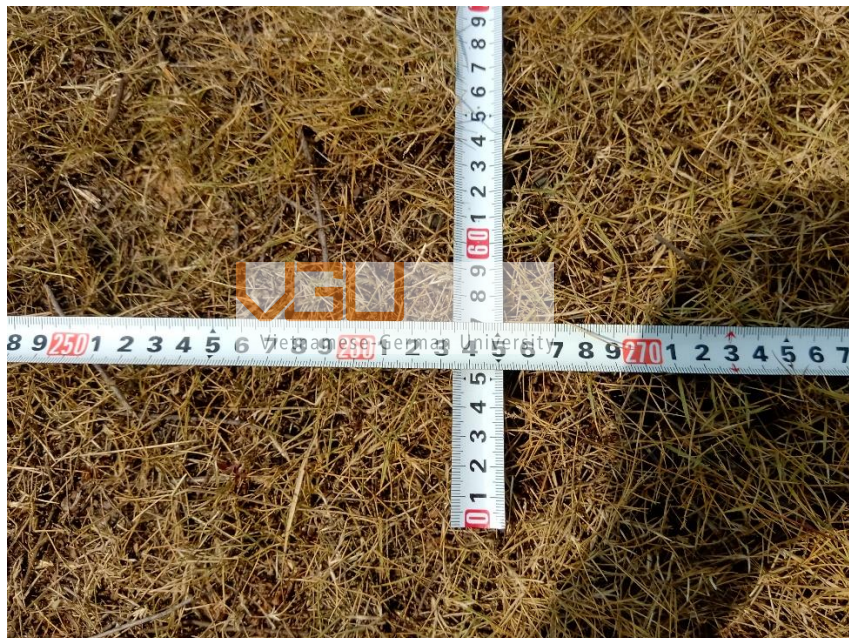
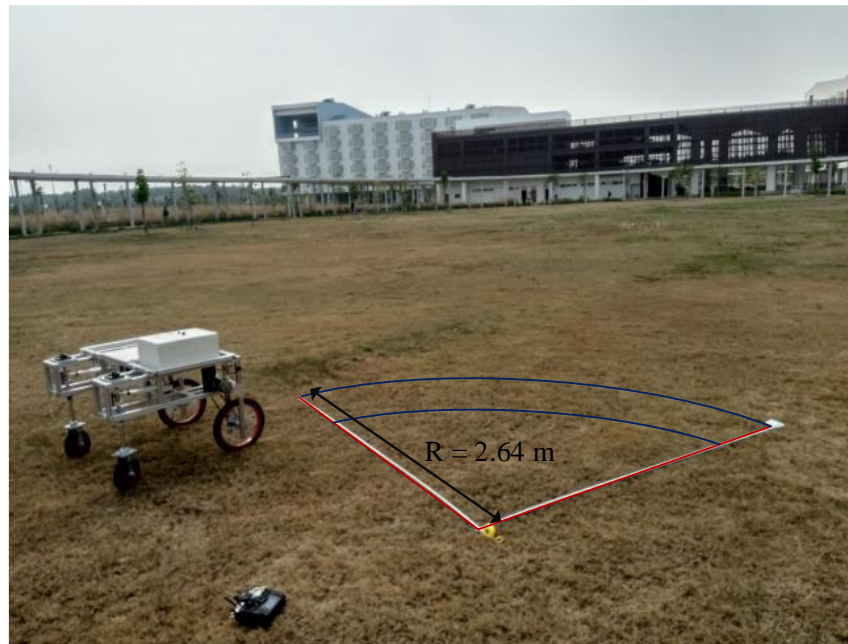


Figure 6.24 2nd steering experiment

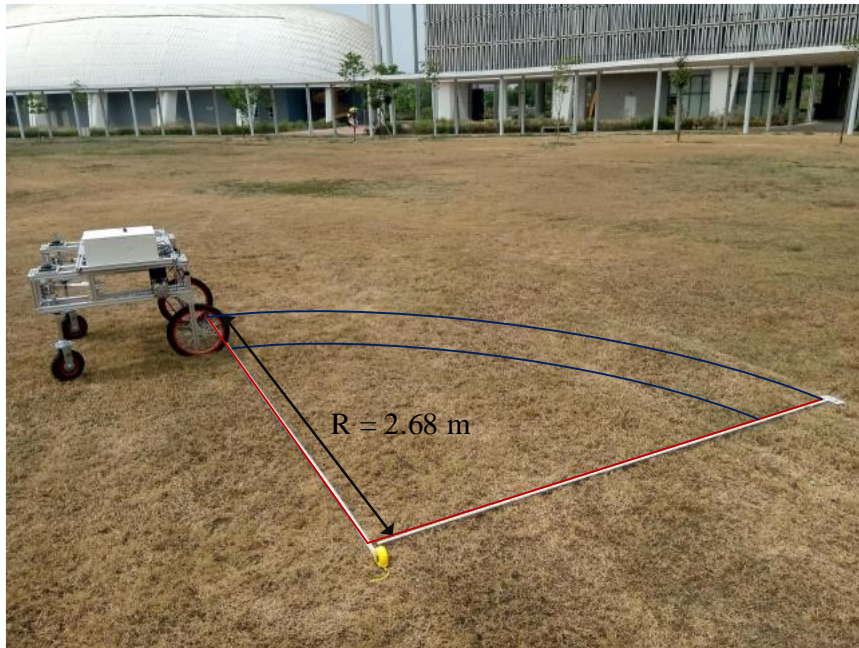


Figure 6.25 3rd steering experiment

Table 6.2 Estimating the steering radius from experiment

	Steering radius
First time	2.83 m
Second time	2.68 m
Third time	2.64 m
Average	$\frac{2.83 + 2.68 + 2.64}{3} = 2.72 \text{ m}$

After conducting experiments, we found that the steering radius of our UGV is larger than what was calculated using the Ackermann formula. There are several reasons for this discrepancy. Firstly, the surface on which the UGV was tested was not ideal, and it had small bumps and uneven terrain which affected the steering performance. Additionally, the steering mechanism of our UGV is not exactly like the Ackermann mechanism due to the use of a parallel steering mechanism, which can lead to differences in steering angles and turning radii. Finally, there may have been some measurement error during the experiment, which can also contribute to the deviation between the experimental and calculated steering radius. Further analysis and experimentation will be conducted to improve the accuracy of the steering system for our agricultural UGV.

7 Conclusion

Based on the research question and objectives, this thesis has successfully designed and developed a prototype of an unmanned ground vehicle (UGV) for collecting data about the height, color, and size of vegetables grown in a plot. The prototype was created with basic mechanical parts and functions, including manual control for movement and turning.

Through the use of Wong's method for driving kinetics, the research estimated the motion resistance caused by the wheel-terrain interaction and determined the motor power needed to choose an appropriate motor. For steering kinetics, another method was used to find the steering resistance moment and determine the power needed for an electric cylinder and select an appropriate electric cylinder. Siemens S7-1500 was selected as the main controller for programming and controlling the motor and electric cylinder.

The research also identified limitations in the design, such as the DC motor and electric cylinder not providing precise control compared to servo or stepper, making it challenging to improve from manual to automatic control. Future research can explore the use of a GPS system with a defined route to enhance automatic control, and the use of servo or stepper motors to improve precision control.

In conclusion, the developed prototype has successfully achieved the research objectives by collecting data about vegetables in the plot. Future research can continue to improve the design to enhance automatic control and precise control, which will be crucial for accurate data collection and analysis.



Appendix

Mathematical code of the calculating the required motor torque in section

```

clc; clear; pi = 3.14; g = 9.81;

% Loam soil properties
n = 0.1;
kc = 5.2;          kc = kc*10^3;          % kN/m^(n+1)      N/m^(n+1)
kphi = 321.11;    kphi = kphi*10^3;        % kN/m^(n+2)      N/m^(n+2)
c = 41;           c = 41*10^3;          % kN/m2           N/m2
phi = 35;         phi = phi*pi/180;      % degrees         pi
gamma = 1.41;     gamma = gamma*13827;    % g/cm3           N/m3
K = 10;           K = K*10^-3;           % mm              m

% UGV
m = 80;           % kg
D1 = 40;          D1 = D1*10^-2;         % cm              m
r1 = D1/2;       % m
bti1 = 4;         bti1 = bti1*10^-2;     % cm              m
pil = 30;         pil = pil*6894.76;        % psi             N/m2
D2 = 20;         D2 = D2*10^-2;         % cm              m
r2 = D2/2;       % m
bti2 = 4;         bti2 = bti2*10^-2;     % cm              m

% Driving kinetics
% General
ad = 0.5;         % m/s2-----
v = 3;           % m/s-----
W_ = m*10;       % N
W = W_/4;        % N
thetas = 5;     thetas = thetas *pi/180; % degree pi
Rg = W_*sin(thetas) % N
If = ad*W_/g     % N
% Motion resistance
pgcr = @(D,bti,pi) (kc/bti+kphi)^(1/(2*n+1))*(3*W/((3-n)*bti*sqrt(D)))^(2*n/(2*n+1));
zr = @(D,bti) (3*W/(bti*(3-n)*(kc/bti+kphi)*sqrt(D)))^(2/(2*n+1));
lt = @(D,zr) sqrt((D/2)^2 - (D/2-zr)^2);
Rc = @(D, bti, b) (1/((3-n)^((2*n+2)/(2+n+1))*(n+1)*bti^(1/(2*n+1))*(kc/b+kphi)^(1/(2*n+1))))*(3*W/sqrt(D))^(2*(n+2)/(2*n+1));
% Bike wheel
pgcr1 = pgcr(D1,bti1,pil); pgcr1_u = pgcr1*0.000145038 % Pa psi
zr1 = zr(D1,bti1); zr1_u = zr1*10^3 % m mm
lt1 = lt(D1, zr1); lt1_u = lt1*10^2 % m cm
if lt1 > bti1
    b1 = bti1; else b1 = lt1; end
Rbike = Rc(D1, bti1, b1)
% Trolley wheel
zr2 = zr(D2,bti2); zr2_u = zr2*10^3 % m mm
lt2 = lt(D2, zr2); lt2_u = lt2*10^2 % m cm
if lt2 > bti2
    b2 = bti2; else b2 = lt2; end
Rtrolley = Rc(D2, bti2, b2)
% Total driving forces
Fd_ = ad*W_/g + 2*Rtrolley + 2*Rbike + Rg; Fd__u = round(Fd_) % N
Fd = Fd_/2 % N
% Motor and tranmision
nt = 90/100; % %

```

```

rsp = 17; % tooth -----
r22 = 14; % tooth -----
nm = 1100; % RPM -----
ww = v/r1
nw = 60*ww/(2*pi)
Mw = Fd*r1/nt
Pm = Mw*nw/9550*1000

% Steering kinetics
% Steering resistance moment
zr = zr2; b = bti2; r = r2;
thetaS = 60; thetaS = thetaS/180*pi; % degrees pi
Xc = pi/4-phi/2; Xc_u = Xc *180/pi % pi degrees
thetal = acos(1-zr/r); thetal_u = thetal *180/pi % pi degrees
MSR11_fun = @(yw, theta) (c + (kc/b+kphi).*r^n.*(cos(theta)-
cos(thetal)).^n.*tan(phi)).*(1 - exp(-
sqrt(r^2.*tan(theta).^2+yw.^2).*abs(thetaS)./K)).*r^2.*tan(theta).^2 ./
sqrt(r^2.*tan(theta).^2+yw.^2);
MSR11 = 2*r* integral2 (MSR11_fun, -b/2, b/2, 0, thetal)
MSR12_fun = @(yw, theta) (c + (kc/b+kphi).*r^n.*(cos(theta)-
cos(thetal)).^n.*tan(phi)).*(1 - exp(-
sqrt(r^2.*tan(theta).^2+yw.^2).*abs(thetaS)./K)).*yw.^2./
sqrt(r^2.*tan(theta).^2+yw.^2);
MSR12 = 2*r* integral2 (MSR12_fun, -b/2, b/2, 0, thetal)
MSR2_fun = @(theta) tan(theta).*(2*c*(r-
r*cos(theta)./cos(theta))./cos(theta)*cot(Xc)+gamma*((r-
r*cos(theta)./cos(theta))./cos(theta)).^2*cot(Xc)^2*(1+cot(Xc)*tan(phi)
));
MSR2 = 2*r^2*cos(thetal)* integral (MSR2_fun, 0, thetal)
MSR = MSR11 + MSR12 + MSR2
% Steering mechanism
Fecxstroke = 2/cot(thetaS)*MSR;
stroke = 100; stroke = stroke*10^-3;
Fec = Fecxstroke/stroke
arm = stroke/sqrt(2*(1-cos(2*thetaS))); arm = arm*100 % cm

```

References

- [1] J. Wong, "6.1 Factors Affecting Off-Road Vehicle Performance," in *Terramechanics and Off-Road Vehicle Engineering, Second Edition: Terrain Behavior, Vehicle Design and Performance*, 2009, pp. 129-130.
- [2] J. Wong, "11.2.1 Rigid Wheel–Terrain Interaction," in *Terramechanics and Off-Road Vehicle Engineering, Second Edition: Terrain Behavior, Vehicle Design and Performance*, 2009.
- [3] J. Wong, "11.2.2 Flexible Tyre–Terrain Interaction - C. Resistance Due to Tyre Flexing," in *Terramechanics and Off-Road Vehicle Engineering, Second Edition: Terrain Behavior, Vehicle Design and Performance*, 2009.
- [4] L. Ding, Z. Deng, H. Gao, J. Guo, D. Zhang and K. D. Iagnemma, ""Experimental study and analysis of the wheels' steering mechanics for planetary exploration wheeled mobile robots moving on deformable terrain,"," *International Journal of Robotics Research*, vol. 32, 2013.
- [5] S. S. S. S. K. P. S. A. M. V. S. R. D. Puneet Gautam, "Designing Variable Ackerman," *International Journal of Analytical, Experimental and Finite Element Analysis*, vol. 8, pp. 1 - 11, 2021.
- [6] R. Jazar, "Vehicle dynamics: Theory and application," *Springer, New York*.
- [7] "Trung tâm Khuyến nông Lâm Đồng," [Online]. Available: <http://khuyennong.lamdong.gov.vn/ky-thuat-trong-trot/ki-thuat-trong-rau>.
- [8] J. Y. Wong, "2.4.1 Characterization of Pressure-Sinkage Relationship," in *Theory of Ground Vehicles*, 2001, p. 136.
- [9] Akbarnia, A. & Mohammadi, A. & Farhani, Foad & Alimardani, R, "Simulation of draft force of winged share tillage tool using artificial neural network model," *Agricultural Engineering International: CIGR Journal*, vol. 16, pp. 57-65, 2014.